

THESIS

SEASONAL SENSITIVITY OF THE EDDY-DRIVEN JET TO TROPOSPHERIC HEATING IN  
AN IDEALIZED ATMOSPHERIC GENERAL CIRCULATION MODEL

Submitted by

Marie C. McGraw

Department of Atmospheric Science

In partial fulfillment of the requirements

For the Degree of Master of Science

Colorado State University

Fort Collins, Colorado

Fall 2015

Master's Committee:

Advisor: Elizabeth Barnes

Thomas Birner

Karan Venayagamoorthy

Copyright by Marie C. McGraw 2015

All Rights Reserved

## ABSTRACT

### SEASONAL SENSITIVITY OF THE EDDY-DRIVEN JET TO TROPOSPHERIC HEATING IN AN IDEALIZED ATMOSPHERIC GENERAL CIRCULATION MODEL

A dry dynamical core is used to investigate the seasonal sensitivity of the circulation to two idealized thermal forcings—a tropical upper tropospheric forcing, and a polar lower tropospheric forcing. The circulation is modified using a set of perpetual simulations to simulate each month of the year, while the thermal forcings are held constant. The circulation responses to tropical warming and polar warming are studied separately, and then the response to the simultaneously applied forcings is analyzed. Finally, the seasonality of the internal variability of the circulation is explored as a possible mechanism to explain the seasonality of the responses. The primary results of these experiments are: 1) There is a seasonal sensitivity in the circulation response to both the tropical and polar forcings. 2) The jet position response to each forcing is greatest in the transition seasons, and the jet speed response exhibits a seasonal sensitivity to both forcings although the seasonal sensitivities are not the same. 3) The circulation response is nonlinear in the transition seasons, but approximately linear in the summer and winter months. 4) The internal variability of the unforced circulation exhibits a seasonal sensitivity that may partly explain the seasonal sensitivity of the forced response. The seasonality of the internal variability of daily MERRA reanalysis data is compared to that of the model, demonstrating that the broad conclusions drawn from this idealized modeling study may be useful for understanding the jet response to anthropogenic forcing.

## ACKNOWLEDGEMENTS

Thanks to my advisor, Professor Elizabeth Barnes for her guidance and support; to the rest of my committee—Professor Thomas Birner and Professor Karan Venayagamoorthy—for their input and assistance; Matt Bishop and Ammon Redman for technical support; and to the rest of the Barnes Research Group (Chengji Liu and Bryan Mundhenk) for their discussion and analysis help. Thanks also to the members of the Thompson, Birner, and Maloney research groups for many thoughtful discussions of atmospheric dynamics and climate. Finally, thanks to Jingyuan Li for assisting me in submitting this thesis in a timely manner.

This thesis is typeset in  $\text{\LaTeX}$  using a document class designed by Leif Anderson.

## TABLE OF CONTENTS

Abstract .....	ii
Acknowledgements .....	iii
List of Tables .....	vi
List of Figures .....	vii
Chapter 1. Introduction .....	1
Chapter 2. Methods .....	9
2.1. Model .....	9
2.2. The Importance of an Imposed Minimum Stratospheric Temperature .....	12
2.3. Control Runs .....	15
2.4. Heating Experiments.....	17
2.5. Adjustment of Mean State .....	19
2.6. Reanalysis Data .....	22
Chapter 3. Results.....	23
3.1. Response of the Model to a Single Thermal Forcing .....	23
3.2. Assessing the Linearity of the Model Response .....	29
3.3. Initial Jet Position Experiments.....	37
Chapter 4. Seasonality of Jet Internal Variability .....	42
4.1. e-Folding Time.....	42
4.2. Spread: A Different Method of Quantifying Internal Variability.....	46
4.3. Comparison with Reanalysis .....	48

Chapter 5. Conclusions .....	52
5.1. Conclusions .....	52
5.2. Future Work .....	54
References .....	59

LIST OF TABLES

2.1 Values of  $\chi$  from equation 2 for every month. .... 11

2.2 Parameters for thermal forcings for TROP, POLAR, and BOTH.  $q_0$  is heating amplitude,  $x_0$  and  $z_0$  are the horizontal and vertical centers of heating, and  $\sigma_x$  and  $\sigma_z$  are the horizontal and vertical half-widths of heating. .... 18

## LIST OF FIGURES

1.1	MERRA monthly reanalysis data showing mean eddy-driven (a) jet position and (b) jet strength for three different basins. Note that the Southern Hemisphere jet position is given in °S, and the Northern Hemisphere jet positions are given in °N.	4
2.1	Comparison of corrected and uncorrected model for (a) June/July temperature, (b) June/July zonal wind, and (c) monthly mean jet position. The dashed lines in (a) and (b) are the corrected temperature and zonal wind contours, and the colors are the anomalies (uncorrected - corrected).	14
2.2	Mean (a) jet position, and (b) strength for model control runs. Error bars indicate the 5th and 95th percentile range to show the internal variability of the jet.	16
2.3	Comparison of jet position (a) and strength (b) responses to polar lower tropospheric heatings centered at various heights (750 hPa and 1000 hPa), and with varying heating thicknesses (125 and 250 hPa).	20
2.4	Comparison of March/October zonal mean temperature profiles (a) prescribed by equation 2.5 and (b) actually output by model. Note that (a) was created with the value of $\chi$ used for March/October in Table 2.1.	21
3.1	Zonal mean (a,b) heating profiles, (c,d) temperature responses, and (e,f) zonal wind responses for the Northern Hemisphere. Dashed lines indicate the temperatures and winds from CTRL, while colors indicate the anomalies for (c,e) TROP and (d,f) POLAR. For (c,d,e,f), the January/December response is shown on the right, and the June/July response is shown on the left. Note that the anomalies for (f) are smaller than those for (e).	24

3.2	(a) Jet position, (b) change in jet position, and (c) change in jet strength for TROP and POLAR heating experiments. ....	26
3.3	Change in (a) jet position and (b) jet strength for BOTH and TROP + POLAR heating experiments. Here, the error bars indicate the confidence bounds on the difference of means between BOTH and TROP+POLAR. ....	31
3.4	(a) Jet position and (b) jet strength as a function of heating rate in March/October. The lines indicates the best fit line for POLAR for values of $q_0 \leq 0$ (dashed line) and $q_0 \geq 0$ (dot-dash line).....	33
3.5	As in Figure 3.4, but for the extended values of heating amplitude ( $q_0$ ).....	36
3.6	(a) Jet position for control runs, and (b) change in jet position for TROP and POLAR heating experiments for mean state experiments (A+5, A+2, and A-2) and model default (DEFAULT). (c) The difference in the jet position response for A+5, A+2, and A-2 compared to DEFAULT. ....	38
4.1	e-folding time ( $\tau$ ) for (a) PC1, (b) jet position, and (c) jet strength for model control runs. Note that the $\tau$ scale for (a) skips from 20 to 50 days. ....	44
4.2	Spread for (a) jet position and (b) jet strength for model control runs. ....	47
4.3	Jet position, jet strength, and PC1 e-folding times for daily MERRA reanalysis data for (a) the North Atlantic, (b) the North Pacific, and (c) the Southern Hemisphere. ....	49

## CHAPTER 1

# INTRODUCTION

One of the most robust signs of climate change is the poleward shift of the midlatitude eddy-driven jets and storm tracks (Collins et al. [14]). The IPCC 5<sup>th</sup> Assessment Report (AR5) states that poleward shifts of the midlatitude eddy-driven jets are likely by the end of the 21st century under the strongest forcing scenario, RCP8.5 (Collins et al. [14]), and Barnes et al. [1] find that all 22 of the CMIP5 (Coupled Model Intercomparison Project, phase 5) models they examined project a poleward shift of the Southern Hemisphere eddy-driven jet by the end of the 21st century (see their Figure 1a). The robustness of the Southern Hemisphere jet response in the CMIP5 and CMIP3 models has been well documented (e.g. Barnes and Polvani [5], Yin [59]). However, there is uncertainty and low confidence in the response of the Northern Hemisphere eddy-driven jet to anthropogenic climate change. This uncertainty is due, in part, to the competing effects of tropical upper tropospheric warming and polar near-surface warming on the midlatitude circulation (e.g. Held [27], [29], Harvey et al. [26], Deser et al. [17]). Thus, a critical component of reducing the uncertainty in the future response of the Northern Hemisphere jet-streams is understanding the circulation response to these low- and high-latitude tropospheric warmings.

Although the earth system response to anthropogenic forcing is and will be comprised of many complex interactions between the atmosphere, ocean, and land surface, the dynamics describing the response of the eddy-driven jet are thought to be likely governed, at least in part, by dry dynamics. Idealized dry models do, in fact, simulate the same sign of the

large-scale response to various climate-change-like warmings as are found in the state-of-the-art climate models (e.g. Tandon et al. [51], Butler et al. [9]). Therefore, idealized models can act as a testbed for exploring the responses of the eddy-driven jet to climate-change-like forcings, and are an efficient and effective way for developing and testing hypotheses that describe the dynamics of these responses. For example, Polvani and Kushner [38] and Kushner and Polvani [31] demonstrate that the eddy-driven jet shifts poleward in response to polar stratospheric cooling in a dry dynamical core; similar to the observed positive trend in the Southern Annular Mode noted by Thompson and Solomon [54] that is attributed to polar stratospheric cooling due to ozone depletion. Wang et al. [56] and Butler et al. [9] note a poleward shift of the eddy-driven jet in response to tropical upper tropospheric heating in a dry dynamical core, consistent with the responses in the current state-of-the-art general circulation models (GCMs) (e.g. Barnes and Polvani [5]). Butler et al. [9] describe the circulation response to three thermal forcings (commonly considered as the signal of anthropogenic warming) in a dry dynamical core—a poleward shift of the storm tracks in response to polar stratospheric cooling and tropical upper tropospheric warming, and an equatorward shift of the storm tracks in response to polar surface warming. They suggest that the mechanisms behind these shifts of the storm tracks are driven by dry dynamics, demonstrating these simple, idealized models can in fact be used to investigate many of the processes driving future changes in the mid-latitude jet-streams.

The eddy-driven jet response to anthropogenic forcing may also be sensitive to the state of the subtropical circulation. The subtropical jet strength can impact the position of the eddy-driven jet (and thus, potentially, the eddy-driven jet response) by controlling the location of the baroclinic region (e.g. Son and Lee [48]). Garfinkel et al. [21] demonstrated that

the magnitude of the jet shift driven by changes in the stratospheric polar vortex strength decreased as the initial jet position was located closer to the subtropics. Since the leading mode of eddy-driven jet variability has been shown to depend on the position and strength of the subtropical jet (e.g. Eichelberger and Hartmann [18], Barnes and Hartmann [3]), and the jet response to external forcing is coupled to its internal variability, it is likely that the state of the subtropical circulation may play a role in determining the zonally symmetric jet response to anthropogenic climate change.

Indeed, the observed eddy-driven jets exhibit distinct seasonal cycles of their own. In Figure 1.1, mean eddy-driven jet positions (Figure 1.1a) and strengths (Figure 1.1b) calculated from the Modern-Era Retrospective Analysis for Research and Applications (MERRA) reanalysis data (Rienecker et al. [39]) are displayed. Here, the eddy-driven jet is defined as the maximum of the vertically-averaged (averaged over 925-700 hPa), low-level zonal mean zonal winds, with a second-order polynomial fit through the maximum. This procedure is described in more detail in Chapter 2. The MERRA data are divided into three different regions, based on the observed storm tracks—the North Atlantic is defined from 15-75°N, 0-70°W (similar to Woollings et al. [58]); the North Pacific, from 15-65°N, 130°E to 120°W (similar to Li and Wettstein [34]); and the Southern Hemisphere, from 15-70°S to 180°E to 180°W.

The seasonal cycles of jet position (Figure 1.1a) are quite different for each basin—the North Pacific exhibits the greatest changes in jet position, ranging from about 36°N in January to about 46°N in August, while the Southern Hemisphere displays the smallest changes in jet position, ranging from about 49°S in June to about 52°S in October (interestingly, this

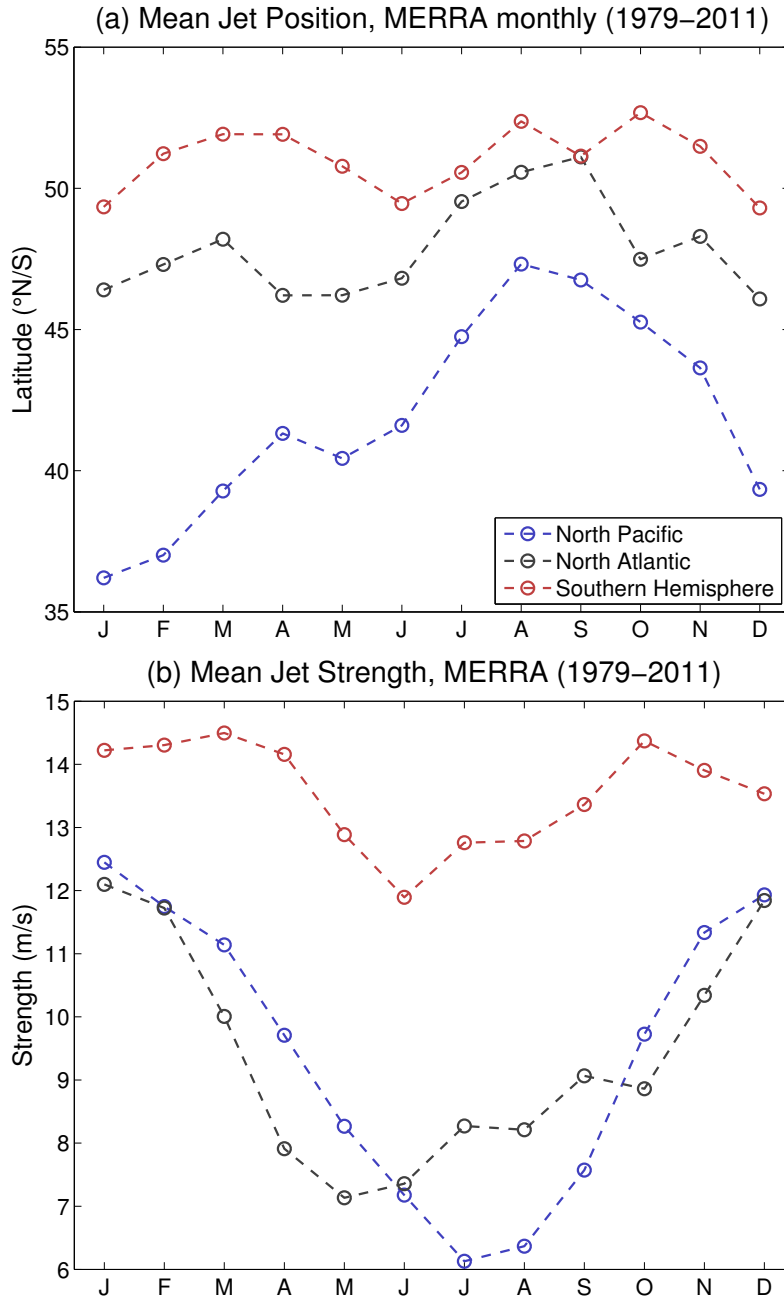


FIGURE 1.1. MERRA monthly reanalysis data showing mean eddy-driven (a) jet position and (b) jet strength for three different basins. Note that the Southern Hemisphere jet position is given in  $^{\circ}\text{S}$ , and the Northern Hemisphere jet positions are given in  $^{\circ}\text{N}$ .

seasonal cycle of the Southern Hemisphere eddy-driven jet is similar to that of the Southern Hemisphere tropical belt width, as seen in Davis and Birner [15]). The jet positions also vary greatly—the North Pacific eddy-driven jet is the most equatorward in all months, while

the Southern Hemisphere eddy-driven jet is most poleward. The seasonal cycles of North Atlantic and North Pacific jet strength (Figure 1.1b) are somewhat similar, with maximum values (around 12-13 m/s) in Northern Hemisphere winter, and minimum values (around 6-7 m/s) in Northern Hemisphere summer, although it is worth noting that the North Atlantic jet strength minimizes in May, while the North Pacific jet strength is at a minimum in July. In the Southern Hemisphere, the jet is actually weakest in Southern Hemisphere winter, although the seasonal cycle of Southern Hemisphere jet strength is much weaker, with the jet strength varying by less than 3 m/s over the course of the year. As these seasonal cycles shown in Figure 1.1 illustrate, these three different basins exhibit substantially different eddy-driven jet behaviors. Differences in the behaviors of different eddy-driven jets have been well-studied previously (for example, Woollings et al. [58] discuss the trimodal behavior of the North Atlantic jet; Williams et al. [57] explore the impacts of the Southern Hemisphere spiral jet on the eddy-driven jet; Lee and Kim [33] and Nakamura and Sampe [36] discuss the influence of the North Pacific subtropical jet on the North Pacific eddy-driven jet; and Li and Wettstein [34] explore differences in the subtropical and eddy-driven jet variability in both Northern Hemisphere basins). This work does not intend to address this topic—these differences are merely pointed out to emphasize that the processes that govern the real eddy-driven jets are complex and highly variable, and that any physical mechanisms proposed through these idealized modeling experiments may not necessarily be capable of fully describing the processes that govern eddy-driven jet behavior in all regions.

It is well known that the strength and position of the eddy-driven jet varies with season in observations (e.g. Figure 1a of Hannachi et al. [25]), as does the variability (e.g. Eichelberger and Hartmann [18], Simpson et al. [47]). Additionally, the strength of the subtropical

jet also exhibits a seasonal cycle (e.g. Figure 4 in Davis and Birner [15]). Therefore, it is possible that the seasonality of the jet dynamics throughout the year could alone drive seasonality in the jet response to climate change. However, previous atmosphere-only GCM (AGCM) studies on the jet response to thermal forcings have tended to focus on the response in a single season—Polvani and Kushner [38], Kushner and Polvani [31], and Wang et al. [56] focus solely on winter, while Butler et al. [9] primarily focus on the equinoctial state (although they do briefly explore the wintertime response). Kushner and Polvani [32] explore the sensitivity of the tropospheric response to a stratospheric seasonal cycle, but do not apply a seasonal cycle to the troposphere. Deser et al. [16] explore the seasonality of the atmospheric response to projected sea ice loss using an AGCM coupled to a land surface model, but they hold greenhouse gas concentrations constant, and force the model with seasonal variations in sea ice and sea surface temperature (SST). Thus, although Barnes and Polvani [5] note that the Northern and Southern Hemisphere jet shifts under RCP8.5 vary seasonally by over  $1^\circ$  across seasons, it is unclear how much of this seasonality is due to the seasonality of the jet dynamics, and how much is due to seasonality of the forcing.

In this work, the seasonality of the circulation response to two idealized thermal forcings is investigated using a dry dynamical core. The first of these is a tropical upper tropospheric warming, intended to simulate the effects of increased heating in the upper tropical troposphere due to anthropogenic forcing. Simply put, the Clausius-Clapeyron describes an increase in equilibrium vapor pressure with increasing global temperature. This increase in water vapor increases the atmosphere’s absorption of solar radiation (the greenhouse effect), creating a positive feedback. The second of these heatings is a polar lower tropospheric warming, meant to simulate Arctic amplification—that is, the preferential warming of the Arctic

when compared to the global mean surface temperature increase due to climate change (e.g. Holland and Bitz [29]). Arctic amplification arises from an increase in poleward heat transport due to increases in global temperature, and is enhanced by reductions in albedo due to reduced snow and ice cover. This work focuses on these two heatings, as the uncertainty in the projections of the Northern Hemisphere circulation response is in large part due to the opposing signs of the responses to upper tropical tropospheric heating and Arctic amplification (e.g. Harvey et al. [26]). The experiments presented here are set up such that the heatings are held constant throughout the simulations, while the tropospheric circulation is given a seasonal cycle by varying the tropospheric relaxation temperature. Although these thermal forcings do in fact vary seasonally in reality, particularly Arctic amplification (e.g. Deser et al. [16]), this framework allows for the separation of seasonal variations in the heating from the seasonal sensitivity of the circulation response to the heating.

These simulations have been run with 20 vertical levels and tropospheric dynamics only. While stratospheric dynamics, and stratosphere-troposphere coupling do affect tropospheric jet dynamics and variability (e.g. Thompson and Birner [53], Butler et al. [8], Polvani and Kushner [38]), stratospheric dynamics are not thought to be the primary driver of the tropospheric jet response to anthropogenic forcing. Simpson et al. [45] and Garfinkel et al. [21] point out that the tropospheric jet response to anthropogenic forcing is primarily governed by tropospheric dynamics (e.g. the strength of tropospheric eddy-mean flow feedbacks, changes in eddy momentum fluxes, and the strength of jet persistence). A more complete discussion of this topic can be found in Section 5 of Garfinkel et al. [21]. Therefore, it is not unreasonable to focus primarily on the tropospheric response and circulation. Furthermore, several previous studies (e.g. Kushner and Polvani [32], Sheshadri et al. [43]) have already explored

the impacts of the stratospheric seasonal cycle and seasonal variability of the polar vortex strength on the tropospheric circulation, and so, the experiments described here have been designed to evaluate the role of the tropospheric circulation's seasonal sensitivity in isolation.

The model and experimental framework are discussed in section 2. Section 3 describes the circulation response to the individual thermal forcings; the circulation response to the combination of both forcings; and the sensitivity of the results to the initial position of the eddy-driven jet. Section 4 explores a possible explanation for the seasonality of the circulation response, and briefly compares the model results to observations. Section 5 presents the conclusions of this work.

## CHAPTER 2

# METHODS

### 2.1. MODEL

All experiments performed in this study use the Geophysical Fluid Dynamics Laboratory (GFDL) spectral dry dynamical core. A dry dynamical core is a model that simply consists of the dry primitive equations of atmospheric motion solved numerically on a rotating sphere. Although a dry core lacks many of the essential components of the atmospheric motions observed in the real world (moisture, clouds, atmosphere-ocean coupling, diabatic processes, and so on), it gives a framework for testing hypotheses based only on the physics of an atmosphere on a rotating Earth. While the results in this study should not be directly compared to results derived from observations or from full general circulation models (GCMs), they can provide a great deal of physical insight regarding atmospheric dynamics. Additionally, these experiments and their subsequent results allow for the formation of more detailed and robust hypotheses that can be tested in models with more advanced physics, ranging from aquaplanets to fully coupled GCMs.

As previously stated, the GFDL dry dynamical core solves the dry hydrostatic primitive equations on a rotating sphere in  $\sigma$  coordinates. The model is run at T42 resolution with 20 evenly spaced sigma levels, and a time step of 1200 sec. Zonal wind and temperature data in both daily and monthly (defined as 30-day means) temporal resolutions are analyzed here. Except where indicated, results are calculated using monthly data. The model configuration is zonally and hemispherically symmetric and is run without topography (there are no topographically-forced stationary waves in this model); therefore, only results for the

Northern Hemisphere will be shown. Model parameters are identical to those used in Held and Suarez [28], referred to as HS94, except where noted.

To simulate radiative processes, HS94 define the model’s Newtonian relaxation temperature profile as,

$$(2.1) \quad T_{eq}^{trop}(p, \phi) = \max \left[ 200 \text{ K}, (T_0 - \delta T_{HS94}) \left( \frac{p}{p_0} \right)^\kappa \right],$$

with  $T_0 = 315\text{K}$ , and  $p_0 = 1000 \text{ hPa}$ .  $\max$  is a maximum function which does not allow the atmospheric temperature to drop below 200 K. This is especially important in the upper levels of the model—since this model configuration does not have realistic stratospheric dynamics, the  $\max$  function largely determines the temperature above the tropopause. The importance of the 200 K minimum temperature is discussed in more detail in the next section. As in Polvani and Kushner [38],  $\delta T_{HS94}$  is modified from HS94 in order to simulate a seasonal cycle, namely, by introducing a hemispheric asymmetry in the radiative equilibrium temperature,

$$(2.2) \quad \delta T_{HS94} = (\Delta T)_y \sin \phi^2 + \epsilon \chi \sin \phi + (\Delta T)_z \log \left( \frac{p}{p_0} \right) \cos \phi^2,$$

where  $\phi$  is the latitude in degrees,  $(\Delta T)_y = 60\text{K}$ ,  $(\Delta T)_z = 10\text{K}$ , and  $\epsilon$  determines the magnitude of the hemispheric asymmetry. The amplitude of  $\epsilon$  is set to 20 K, following Chen and Plumb [13]. Increasing the amplitude of  $\epsilon$  from the often-used value of 10 K (e.g. Polvani and Kushner [38]) has the dual effect of enhancing the hemispheric asymmetry and improving the basic state of the model, by producing a stronger subtropical jet and a more poleward eddy-driven jet than when  $\epsilon = 10 \text{ K}$ .  $\chi$  is a multiplier that modifies the value of  $\epsilon$  based on the season. At the Northern Hemisphere winter solstice, when the asymmetry

TABLE 2.1. Values of  $\chi$  from equation 2 for every month.

Month	$\chi$	Month	$\chi$
JAN	+0.9659	JUL	-0.9659
FEB	+0.7071	AUG	-0.7071
MAR	+0.2588	SEPT	-0.2588
APR	-0.2588	OCT	+0.2588
MAY	-0.7071	NOV	+0.7071
JUN	-0.9659	DEC	+0.9659

between the two hemispheres is greatest,  $\chi$  is set to 1 (and  $\chi = -1$  for Northern Hemisphere summer). On the equinoxes, when the asymmetry between the two hemispheres is zero,  $\chi$  is set to 0. Many previous studies have run this model under solstice conditions, so  $\chi$  is assumed to be 1 and is not explicitly mentioned in those studies. Here,  $\chi$  is varied to simulate a seasonal cycle. Six different values of  $\chi$  were chosen to simulate six months of the year; the other six months were assumed to be identical. So, although only six separate values of  $\chi$  were simulated, the results are presented in 12 month format to visualize the full seasonal cycle. The values of  $\chi$  used for each month are listed in Table 2.1.

## 2.2. THE IMPORTANCE OF AN IMPOSED MINIMUM STRATOSPHERIC TEMPERATURE

Recall the equation for the tropospheric equilibrium temperature profile is,

$$(2.3) \quad T_{eq}^{trop}(p, \phi) = \max \left[ 200K, \left( T_0 - \left( (\Delta T)_y \sin \phi^2 + \epsilon \sin \phi + (\Delta T)_z \log \left( \frac{p}{p_0} \right) \cos \phi^2 \right) \right) \left( \frac{p}{p_0} \right)^\kappa \right],$$

Equation 2.3 specifies that  $T_{eq}^{trop}$  cannot be lower than 200 K. However, in the posted current version of the GFDL dry dynamical core (available at [http://data1.gfdl.noaa.gov/~arl/pubrel/m/atm\\_dycores/](http://data1.gfdl.noaa.gov/~arl/pubrel/m/atm_dycores/)), this lower bound on the temperature (here called  $T_{min}$ ) is allowed to vary with season,

$$(2.4) \quad T_{min} = 200 - \epsilon \sin \phi$$

For example, for  $\epsilon = 20K$  and  $\phi = 90^\circ$  (winter solstice at the North Pole),  $T_{min}$  would be 180 K. This seasonal variation allows the upper levels in the winter hemisphere to cool below 200 K, which shifts the eddy-driven jet slightly poleward. However, the greater impact of this variation occurs in the summer hemisphere, which is allowed to warm excessively, as seen in Figure 2.1, which compares the uncorrected ( $T_{min}$  varies with season, as in equation ) and corrected ( $T_{min}$  cannot drop below 200 K, as in equation (2.3)) model temperature profiles. This excessive stratospheric warming shifts the summer hemisphere jet much too far equatorward—in some months, as much as  $10^\circ$ , as seen in Figure 2.1b. This large equatorward bias in the summer jet position also results in an opposite seasonal cycle of the jet. In Figure 2.1c, the uncorrected jet (open circles) is most poleward in winter and most equatorward in summer, which is in opposition to observations (e.g. Figure 1.1 in Chapter 1). The corrected jet (closed circles), on the other hand, exhibits a jet seasonal cycle that is comparable to the observed jet seasonal cycle. This issue only affects the troposphere-only

model configuration—when the model is run with a stratosphere, the temperature is not constrained by the maximum function in equation 2.3, as the presence of stratospheric dynamics allows the model to set its own temperature (see Polvani and Kushner [38] and Kushner and Polvani [32] for more details about the stratospheric dynamics).

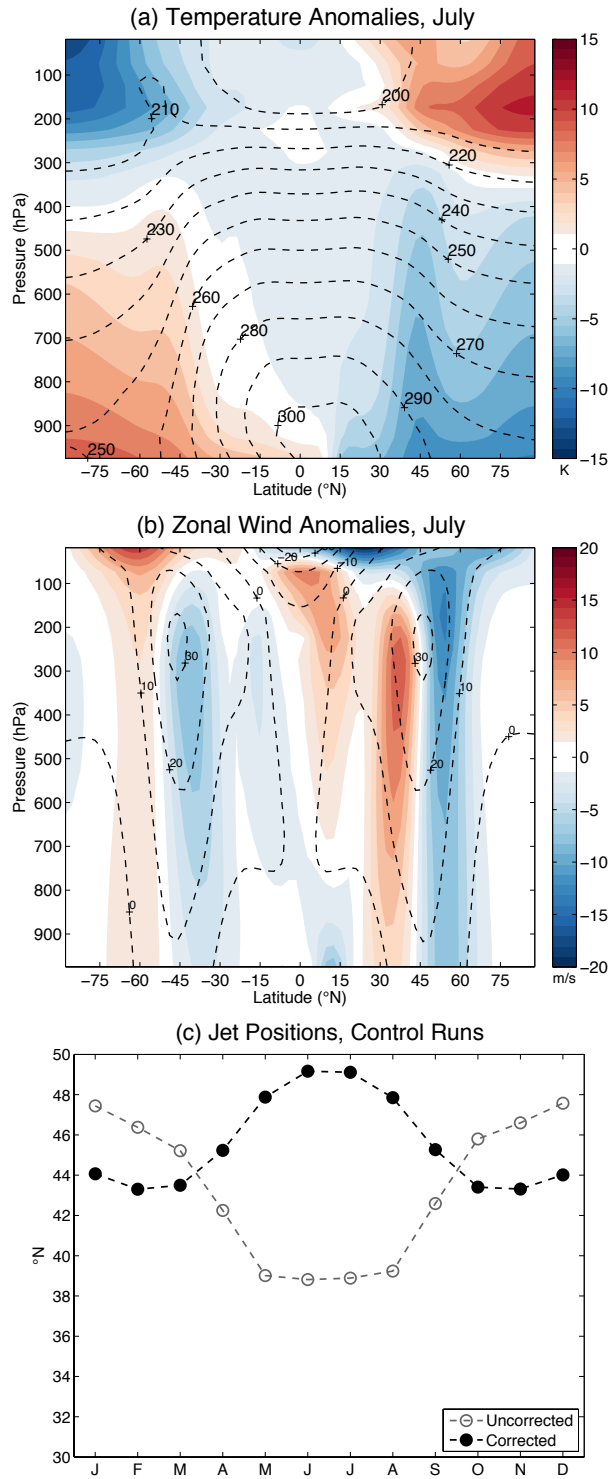


FIGURE 2.1. Comparison of corrected and uncorrected model for (a) June/July temperature, (b) June/July zonal wind, and (c) monthly mean jet position. The dashed lines in (a) and (b) are the corrected temperature and zonal wind contours, and the colors are the anomalies (uncorrected - corrected).

### 2.3. CONTROL RUNS

The first family of experiments uses the model default configuration, described in (2.1) and (2.2). For each experiment, each month is run separately under perpetual conditions (i.e. perpetual January, perpetual February, etc.). While perpetual simulations are perhaps not wholly realistic outside of the solstices (the times of year when the rate of change of the solar forcing is very small), transient runs simulating a full seasonal cycle were briefly examined (not shown), and the results from these simulations are qualitatively similar to the perpetual simulations. For each of the six values of  $\chi$  seen in Table 2.1, two separate 50 year simulations are run and then averaged together. Thus, each experiment is actually comprised of twelve separate simulations, two for each value of  $\chi$ . First, two 50 year control experiments (referred to as CTRL) with no heating are run for each value of  $\chi$ , with the first two years discarded for spin-up. The heating experiments, described in detail in the next section, branch off of these control runs, and follow the same structure of two 50 year runs for each value of  $\chi$  that are subsequently averaged together.

In all experiments, the primary variables of interest are the eddy-driven jet position and strength. As is common practice, the jet position is defined by identifying the maximum of the zonal mean zonal wind near the surface, and then fitting a second-order polynomial through the maximum. The location and magnitude of the maximum of the polynomial are the jet position and strength, respectively. This quantity is often calculated for observational data by averaging over several pressure levels (e.g. Woollings et al. [58]); in these simulations, the vertically averaged results are almost identical to the results obtained using only 775 hPa. Thus, only a single pressure level is used for simplicity.

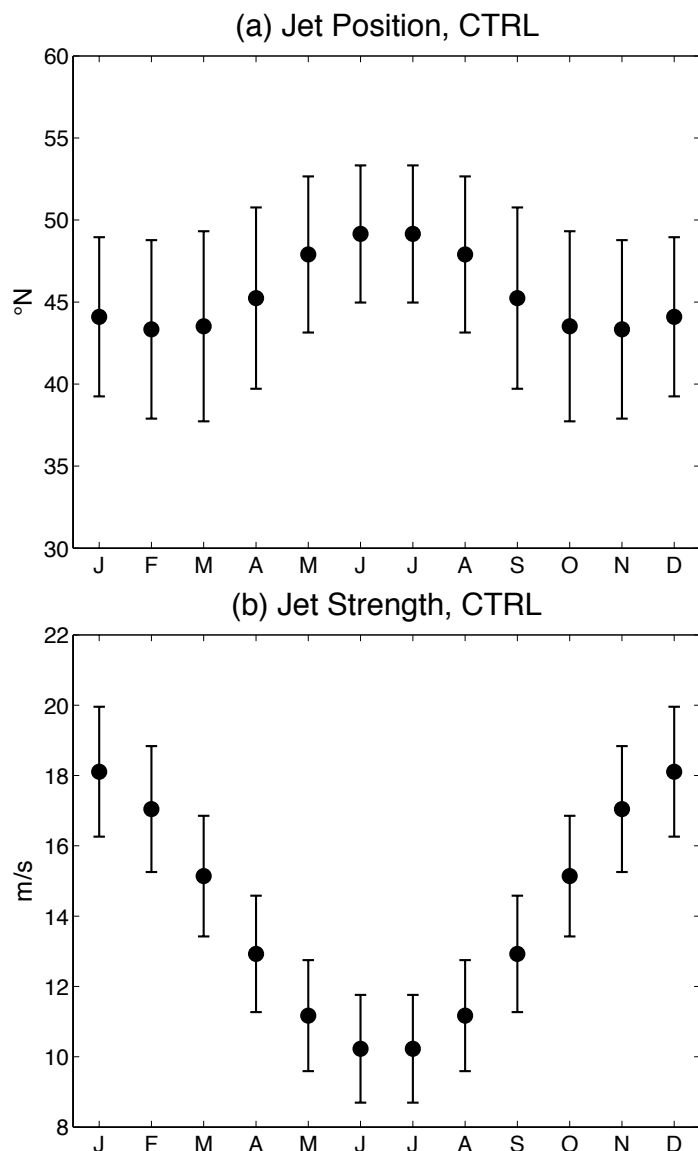


FIGURE 2.2. Mean (a) jet position, and (b) strength for model control runs. Error bars indicate the 5th and 95th percentile range to show the internal variability of the jet.

The mean jet position and strength for each month’s control run (CTRL experiment) are shown in Figure 2.2. As seen in Figure 2.2a, the jet is positioned more poleward in summer than in winter. The jet position is located between 40°N and 50°N. This latitude range is comparable to the observed mean monthly latitudes of the North Atlantic and Southern Hemisphere eddy-driven jets (see Figure 1.1a in Chapter 1). The mean jet strength, seen in Figure 2.2b, is strongest in the winter, when temperature gradients are strongest and

baroclinicity is greatest, and weakest in the summer, when temperature gradients and baroclinicity are weakest. The jet strengths vary from about 18 m/s to about 10 m/s. Again, these values are comparable to the observed jet strengths (see Figure 1.1b in Chapter 1).

## 2.4. HEATING EXPERIMENTS

At the end of each month's control simulation, two thermal forcing experiments are applied to the model. The first experiment, TROP, simulates the tropical upper tropospheric warming due to increased latent heating of water vapor (a signature of greenhouse gas warming) (see Figure 12 in Collins et al. [14]). The second experiment, POLAR, simulates the polar lower tropospheric warming associated with Arctic amplification (e.g. Holland and Bitz [29]). The heating experiments branch off of the end of the control runs and run for another 50 years, with the first two years discarded for spin-up. So, the January tropical heating experiment branches off at the end of the January control experiment, and so on. The thermal forcings are turned on at the beginning of the runs, and remain constant throughout the simulations. Most importantly, the strength and location of the heating is identical in every month.

Following Butler et al. [9], the zonally symmetric forcing,  $F$ , is defined as,

$$(2.5) \quad F = q_0 \exp \left\{ - \left[ \frac{(x - x_0)^2}{2\sigma_x^2} + \frac{(z - z_0)^2}{2\sigma_z^2} \right] \right\},$$

where  $q_0$  is the amplitude of heating,  $x$  is the latitude (in radians), and  $z$  is the sigma level. Thus, the heating is Gaussian in  $x$  and  $z$ . The heating amplitude,  $q_0$ , is different for TROP (0.3 K/day) and POLAR (0.5 K/day), and does not vary unless otherwise noted. The POLAR heating amplitude is larger than the TROP heating amplitude because the Arctic is

projected to warm more relative to other parts of the globe (see Figure 10 in Collins et al. [14], Screen and Simmonds [41]). Additionally, Wang et al. [56] have noted abrupt circulation changes in this model when forced with a very strong tropical upper tropospheric heating, so a slightly lower heating amplitude for TROP was used to avoid these abrupt transitions. For all heating experiments, the additional parameters in equation 2.5 are given in Table 2.2.

TABLE 2.2. Parameters for thermal forcings for TROP, POLAR, and BOTH.  $q_0$  is heating amplitude,  $x_0$  and  $z_0$  are the horizontal and vertical centers of heating, and  $\sigma_x$  and  $\sigma_z$  are the horizontal and vertical half-widths of heating.

Experiment name	$q_0$ (K/day)	$x_0 \pm \sigma_x$ ( $^\circ$ )	$z_0 \pm \sigma_z$ (hPa)
TROP	0.3	$0 \pm 27$	$300 \pm 125$
POLAR	0.5	90 - 16	$750 \pm 125$
POLAR <sub>surf</sub>	0.5	90 - 16	$1000 + 125$
POLAR <sub>thick</sub>	0.5	90 - 16	$1000 + 250$
BOTH	0.3	$0 \pm 27$	$300 \pm 125$
	0.5	90 - 16	$750 \pm 125$

The zonal mean heating profiles for TROP and POLAR are plotted in Figure 3.1a and Figure 3.1b in Chapter 3, respectively. The heating in the TROP experiment (Figure 3.1a) represents the signature of greenhouse gas warming—a rise in temperatures in the tropical upper troposphere due to increased water vapor. The POLAR experiment simulates Arctic amplification—the lower-level polar warming attributed, in part, to the ice-albedo feedback of the Arctic (e.g. Screen and Simmonds [41]). The vertical center of heating for POLAR (Figure 3.1b) is not at the surface, as is seen in the observed Arctic warming (see Figure 1 in Screen and Simmonds [41]). Instead, the heating is centered in the lower troposphere, at 750 hPa. This heating profile is not intended to exactly mimic observed Arctic amplification solely due to the loss of sea ice—instead, the heating is positioned in order to extend well beyond the boundary layer, where it is more able to significantly impact the large-scale

circulation. Similar experiments were run with the POLAR heating positioned at the surface, which more closely resembles observed Arctic warming. As seen in Figure 2.3, the response retained the same seasonal sensitivity and differed only in amplitude from the POLAR experiment presented here.

## 2.5. ADJUSTMENT OF MEAN STATE

The second set of experiments tests the seasonal sensitivity of the jet response to the climatological position of the jet. The mean jet position is varied by further modifying the background equilibrium temperature profile in a manner consistent with previous studies (e.g. Simpson et al. [44], Garfinkel et al. [21]). These modifications to the background equilibrium temperature profile change the mean meridional position of the jet without having a large impact on the jet speed or eddy heat and momentum fluxes. To do this, the  $\delta T_{HS94}$  term (equation (2)) is modified further, following Garfinkel et al. [21],

$$(2.6a) \quad \delta T_{new} = \delta T_{HS94} + A \cos [2(\phi - 45)]P(\phi),$$

$$(2.6b) \quad T_{eq}^{trop}(p, \phi) = \max \left[ 200 \text{ K}, (T_0 - \delta T_{new}) \left( \frac{p}{p_0} \right)^\kappa \right],$$

where  $P(\phi) = \sin [4(\phi - 45)]$ , and  $\phi$  is latitude in degrees. Note that the full equation used by Garfinkel et al. [21] includes a third term that depends on a parameter,  $B$ . However, as  $B$  is set to zero throughout this study, that term has been dropped from equation for simplification. Increasing  $A$  shifts the jet poleward, and decreasing  $A$  shifts the jet equatorward. While the shape of the equilibrium temperature profile changes slightly (see Figure 2 in Garfinkel et al. [21]), and Figure 2.4, the equator-to-pole temperature difference does not change.

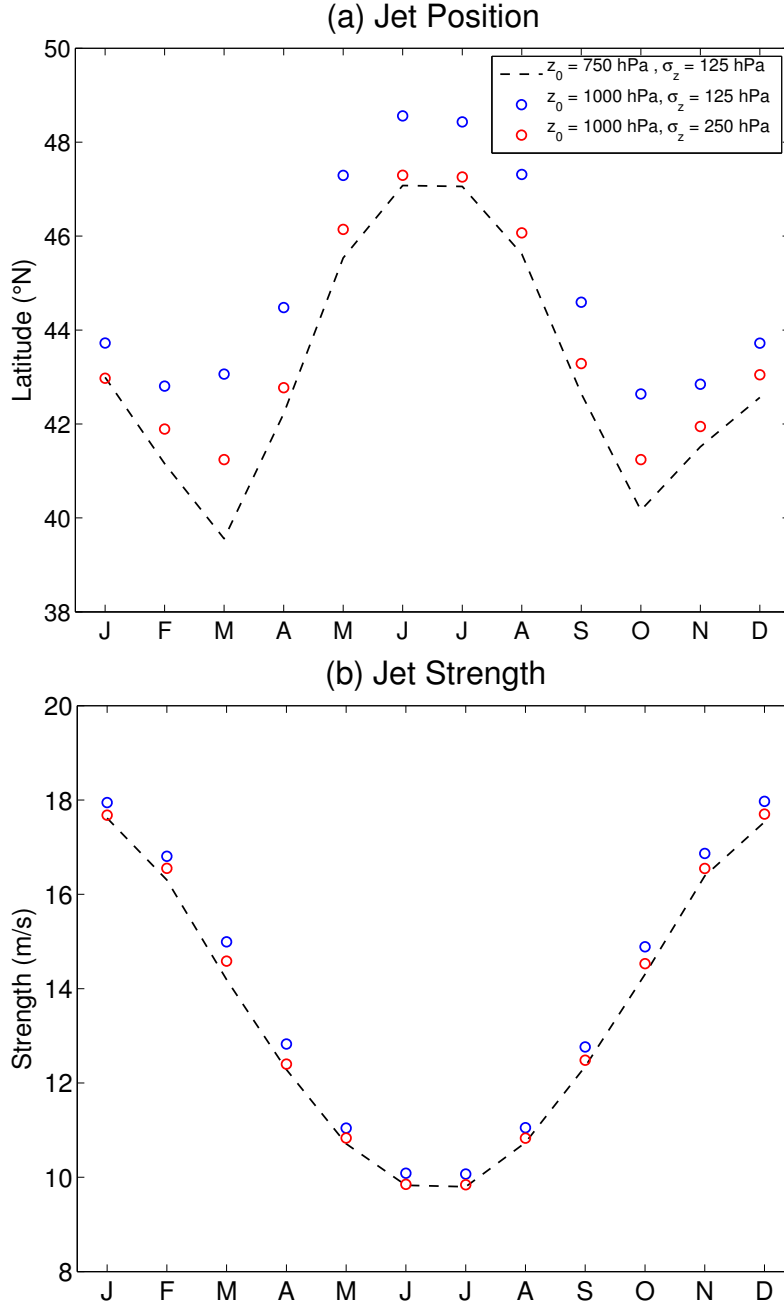


FIGURE 2.3. Comparison of jet position (a) and strength (b) responses to polar lower tropospheric heatings centered at various heights (750 hPa and 1000 hPa), and with varying heating thicknesses (125 and 250 hPa).

Four different values of  $A$  were tested in this set of experiments:  $A = \pm 5.0$ , referred to as  $A + 5$  and  $A - 5$ , respectively; and  $A = \pm 2.0$ , referred to as  $A + 2$  and  $A - 2$ , respectively.  $A + 5$  is similar to the GCM49 experiment in Barnes and Thompson [6], and  $A + 2$  and  $A - 2$

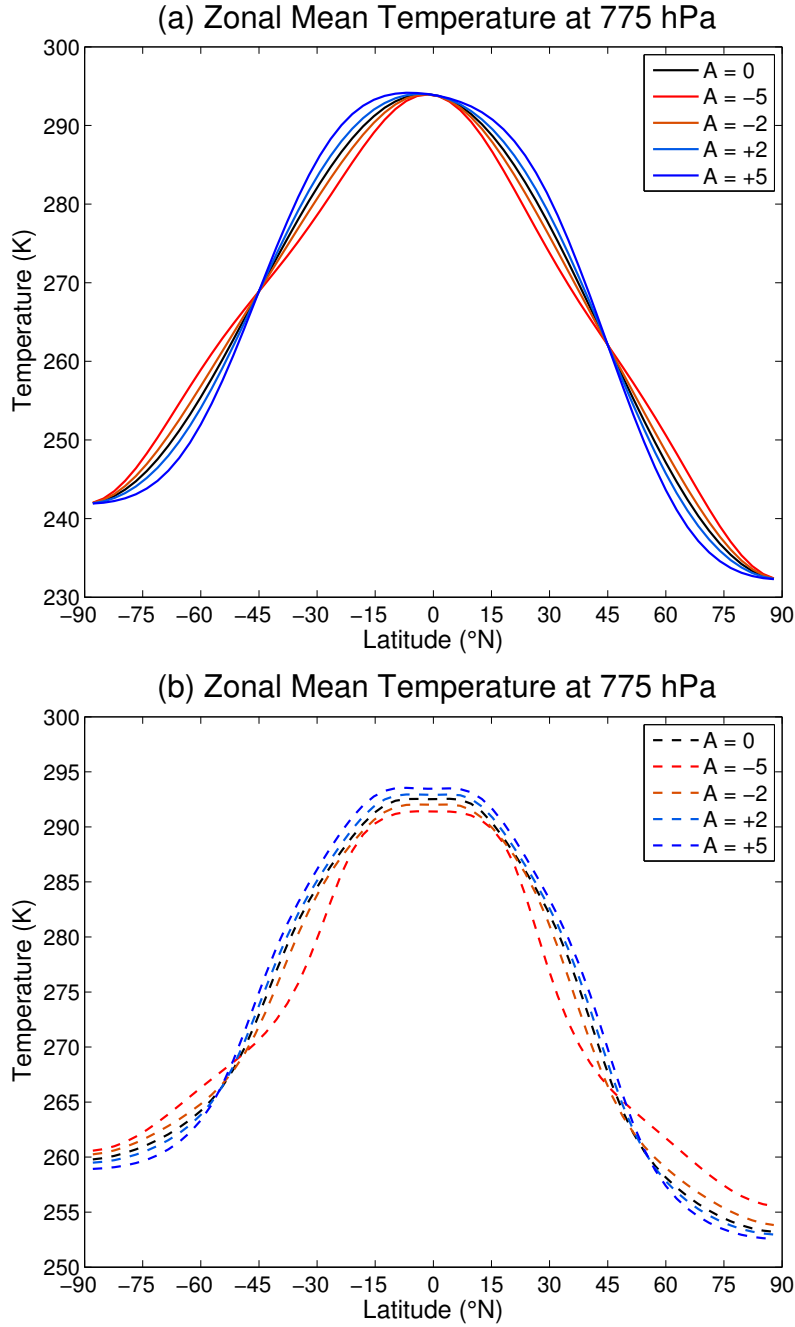


FIGURE 2.4. Comparison of March/October zonal mean temperature profiles (a) prescribed by equation 2.5 and (b) actually output by model. Note that (a) was created with the value of  $\chi$  used for March/October in Table 2.1.

are similar to the TR4 and TR2 experiments in Simpson et al. [44]. Each of these four experiments is also initiated with two separate 50 year control runs for each value of  $\chi$ . Similar to the first set of experiments, the TROP and POLAR heat forcings described in

Table 2.2 are applied at the end of each control run, and run for an additional 50 years. The results of these mean state experiments are then compared to the first set of experiments to determine the sensitivity of the circulation response to the mean position of the jet.

## 2.6. REANALYSIS DATA

In the final part of this study, the daily Modern-Era Retrospective Analysis for Research and Applications (MERRA) reanalysis data (Rienecker et al. [39]) is used to compare the idealized modeling results with observations. The MERRA data used here have a horizontal spatial resolution of  $1.25^\circ \times 1.25^\circ$ . For simplicity, this analysis is restricted to the North Atlantic region, which is defined as extending from  $15\text{-}75^\circ$  N and  $0\text{-}70^\circ$  W. In this study, the daily zonal wind (U) from January 1979 to December 2010 is vertically averaged over four levels—925, 850, 775, and 700 hPa—and used to calculate the eddy-driven jet position and strength using the method described in Section 2b. As in previous studies (e.g. Woollings et al. [58]), a 10-day Lanczos filter with 61 weights is applied to the daily data before the jet position and strength are calculated, removing the features associated with higher frequency synoptic variability and preserving only the low-frequency variability of the eddy-driven jet. This 10-day Lanczos filter is also applied to the vertically-averaged zonal wind fields used to calculate the e-folding time of the first principal component time series of the zonal-mean zonal wind (see Chapter 4 for more information about this calculation).

## CHAPTER 3

# RESULTS

### 3.1. RESPONSE OF THE MODEL TO A SINGLE THERMAL FORCING

The Northern Hemisphere zonal mean temperature (Figure 3.1c and Figure 3.1d) and zonal wind (Figure 3.1e and Figure 3.1f) responses to the TROP and POLAR experiments are shown in Figure 3.1. The TROP experiments are shown on the left (Figure 3.1c, Figure 3.1e), and the POLAR experiments are shown on the right (Figure 3.1d and Figure 3.1f). For Figures 3.1c-f, the January/December response is shown on the right, and the June/July response is shown on the left side of each panel. For the TROP experiment, the difference between the temperature response (Figure 3.1c) in January/December (right) and June/July (left) is small. The largest temperature response is seen where the heating is applied in the tropical upper troposphere, and the response elsewhere is weaker. In the POLAR experiment, the temperature response (Figure 3.1d) is also greatest where the heating is applied in both June/July (left) and January/December (right), and is negligible outside of this region.

The zonal wind responses for TROP (Figure 3.1e) and POLAR (Figure 3.1f), however, do exhibit responses throughout the troposphere. For example, the zonal wind response for TROP (Figure 3.1e) shows a poleward shift in the eddy-driven jet (indicated by the positive zonal wind anomalies centered around  $60^{\circ}\text{N}$ ) in both January/December (right) and June/July (left). These positive zonal wind anomalies extend vertically throughout the troposphere. The zonal wind response in POLAR (Figure 3.1f) shows an equatorward shift of the jet in both June/July (left) and January/December (right), indicated by the negative anomalies centered around  $55^{\circ}\text{N}$  and the positive anomalies centered around  $30^{\circ}\text{N}$ . Note that

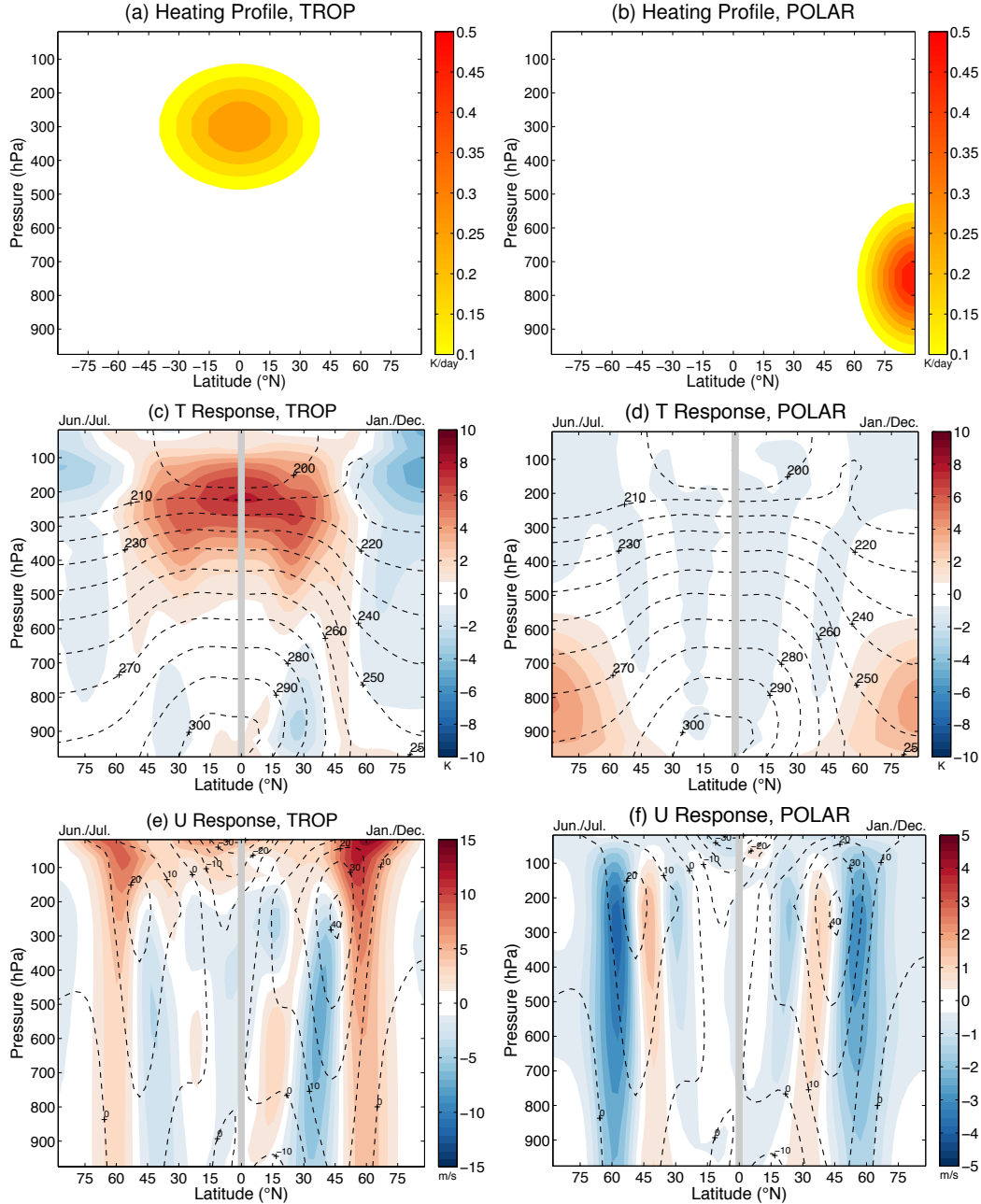


FIGURE 3.1. Zonal mean (a,b) heating profiles, (c,d) temperature responses, and (e,f) zonal wind responses for the Northern Hemisphere. Dashed lines indicate the temperatures and winds from CTRL, while colors indicate the anomalies for (c,e) TROP and (d,f) POLAR. For (c,d,e,f), the January/December response is shown on the right, and the June/July response is shown on the left. Note that the anomalies for (f) are smaller than those for (e).

the zonal wind anomalies due to the tropical upper tropospheric heating (Figure 3.1e) are larger than those induced by the polar lower tropospheric heating (Figure 3.1f).

The zonal wind responses to the two imposed heatings—a poleward shift in response to TROP, and an equatorward shift in response to POLAR—have been previously observed in many studies (e.g. Ring and Plumb [40], Butler et al. [9]). The sign of this response is often attributed to meridional changes in the temperature field. For example, imposing a heating in the tropical upper troposphere would be expected to warm the tropical atmosphere at upper levels, while the polar atmosphere at the same vertical heights would not be expected to warm. This would increase the horizontal equator-to-pole temperature difference, which would increase the upper level winds based on thermal wind balance. Chen and Held [12] hypothesize that this increase in the upper level winds would increase the Rossby wave phase speed, which would shift the eddy momentum flux convergence (and thus, the eddy-driven jet) poleward. The equatorward shift of the jet in response to a polar low-level warming is suggested to be a response to changes in lower-level baroclinicity due in part to changes in the lower-level equator-to-pole temperature gradient caused by the polar warming (e.g. Deser et al. [16]).

For all following analysis, the midlatitude circulation is quantified as the response of the midlatitude jet position and strength using the metrics described previously. The monthly mean jet positions for TROP and POLAR are compared to those of CTRL in Figure 3.2a. Throughout this study, the responses to the tropical heating are shown in red, while the responses to the polar heating are shown in blue. The seasonal cycle exhibited by the jet in the CTRL experiment is preserved in the heating experiments—in all experiments, the jet is further poleward in summer than in winter. In the TROP experiment, the jet position seasonal cycle is flatter than that of CTRL—that is, the difference between the most poleward and most equatorward months is smaller in the TROP experiment than it is in

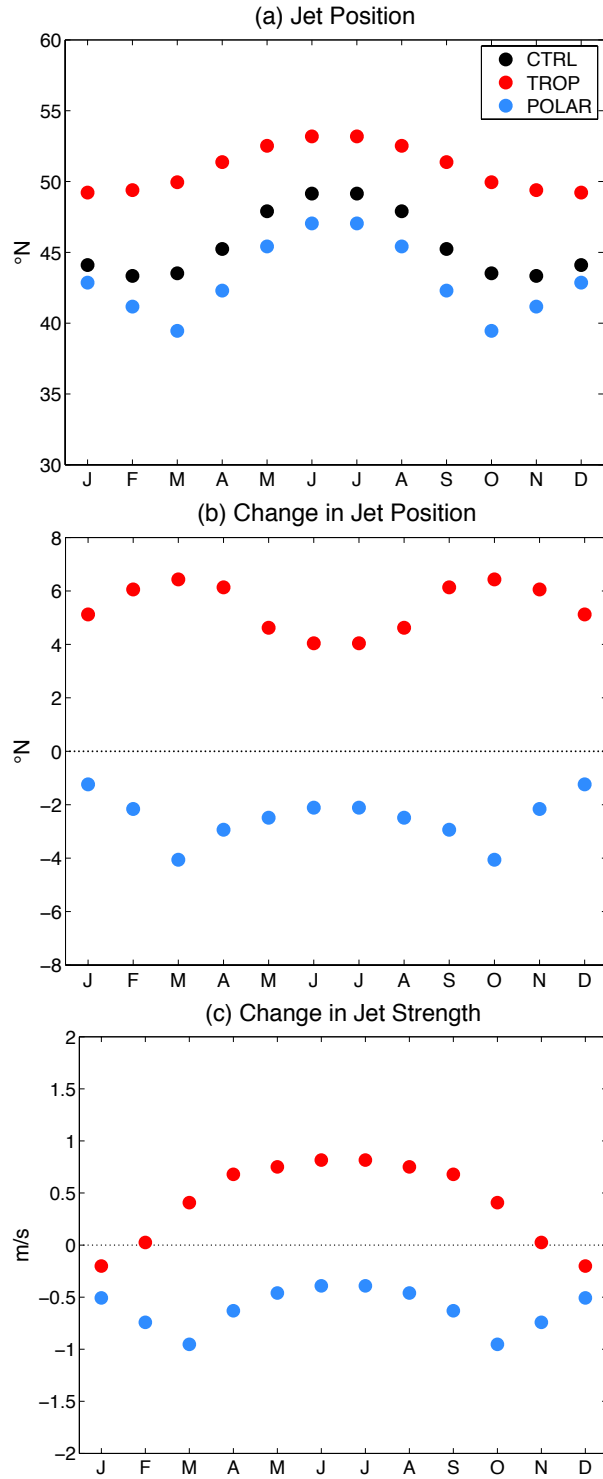


FIGURE 3.2. (a) Jet position, (b) change in jet position, and (c) change in jet strength for TROP and POLAR heating experiments.

the CTRL experiment. In contrast, the seasonal cycle of the jet position is enhanced in the POLAR experiment—the difference between the most poleward month and the most equatorward month is greater for the POLAR experiment when compared to the CTRL experiment.

Figure 3.2b compares the jet position response in the TROP and POLAR experiments. The jet position response is defined as the change in jet position for the heating experiments as compared to the CTRL experiment. Consistent with previous modeling studies (e.g. Butler et al. [9]), the jet shifts poleward in every month in response to a tropical upper tropospheric heating (the TROP experiment), and equatorward every month in response to a polar lower tropospheric heating (the POLAR experiment). However, although the sign of the response is the same, Figure 3.2b clearly indicates that the amplitude of the response to both TROP and POLAR varies across months. Since an identical thermal forcing is applied in each month, these differences in the amplitude of the response show that there is a seasonal sensitivity in the circulation response to tropospheric heating. The amplitude of the circulation response is largest in the transition seasons for both of the heating experiments, with smaller responses occurring in the summer and the winter months. The differences between the months with the largest response (March/October for both TROP and POLAR) and the month with the smallest response (June/July for TROP, January/December for POLAR) exceeds  $3^\circ$  latitude. Many studies evaluate the circulation response to simulated climate change either in the annual mean or in the winter (e.g. Ring and Plumb [40], Butler et al. [9], Polvani and Kushner [38]). However, Figure 3.2b demonstrates that this would lead to an underestimation of the maximum amplitude of the circulation response in this model.

Similar to Figure 3.2b, Figure 3.2c displays the response of the jet strength. The seasonal cycles of jet strength for TROP and POLAR are similar to that of CTRL (not shown; the seasonal cycle of jet strength for CTRL can be seen in Figure 2.2b), with the jet strongest in winter and weakest in summer. However, the jet position and strength responses do not exhibit the same seasonal sensitivity to the TROP experiment. The jet strength changes most in the summer, strengthening by up to 1 m/s. By contrast, the response in the winter months is weak, and even negative (indicating a weakening of the jet) in January/December. The jet strength response to POLAR, however, does have a similar seasonal sensitivity to that of jet position, namely the jet strength response is negative in all months, indicating a weakening of the jet, and is largest in March/October.

The discrepancies between the jet position and strength responses to the simulated greenhouse gas forcing (the TROP experiment) are especially noteworthy for their implications regarding the use of the annular modes to determine the circulation responses to climate change. The Northern Hemisphere circulation response to greenhouse gas forcing is often described as an overall positive trend in the Northern Annular Mode (NAM, often subdivided into the North Atlantic Oscillation (NAO) and the Pacific North American pattern (PNA)) and Southern Annular Mode (SAM) throughout the 21st century (e.g. Gillett and Fyfe [23]). The jet position and jet strength are incorporated together into one measure of the annular mode—for example, a positive NAO event is often characterized by a stronger, more poleward North Atlantic jet, while a negative NAO event is often indicated by a weaker, more equatorward North Atlantic jet (e.g. Woollings et al. [58]). However, as Figure 3.2c demonstrates, the seasonality of the jet position and strength responses to an upper tropical tropospheric warming may not be the same. This difference is particularly strong in winter,

the season most strongly associated with NAO/NAM patterns—the jet actually weakens in December-January, and shows little change in November and February. Therefore, caution must be taken when linking seasonal trends in the annular modes to trends in the jet position and speed, as they do not necessarily vary in the same way (e.g. Swart et al. [50], Thomas et al. [52]).

### 3.2. ASSESSING THE LINEARITY OF THE MODEL RESPONSE

In the real atmosphere, the projected thermal forcings due to climate change do not and will not occur in isolation. That is, the circulation will be forced by both tropical upper tropospheric heating and polar lower tropospheric heating at the same time. Therefore, while it is instructive to study the circulation’s response to these two heatings (represented by the TROP and POLAR experiments) separately, it is also worthwhile to study the linearity of the circulation response to the simultaneous application of TROP and POLAR. In this section, the response to these two concurrent forcings, TROP and POLAR, is compared to the superposition of the responses to individual forcings in order to assess the linearity of the circulation response. The linearity of the circulation response to the strength of the heating is also examined by adjusting the strength of the TROP and POLAR heating amplitudes ( $q_0$ ).

A third experiment, BOTH, was run by applying both the TROP and POLAR heating experiments together (i.e., a simultaneous application of the heatings in Figure 3.1a and Figure 3.1b). If the circulation response to the BOTH experiment is similar to the addition of the TROP and POLAR responses, then the jet response to multiple heating sources would be considered linear—that is, the response can be accurately reconstructed by superimposing the responses of TROP and POLAR separately (referred to as TROP + POLAR). If,

however, the responses of BOTH and TROP + POLAR are not similar, then the circulation response would be considered nonlinear with regard to the heating location. Figure 3.3a demonstrates that, while the responses to BOTH and TROP + POLAR are approximately equal in the winter and the summer months, the response to BOTH is much greater (up to  $3^\circ$  latitude) in the transition seasons than the response to TROP + POLAR. The jet position response to multiple thermal forcings is thus quite nonlinear in the transition seasons. Additionally, note that in every month, the response to BOTH is equal to or larger than the response to TROP + POLAR. The poleward shift of the jet in response to TROP is larger, or, alternatively, the equatorward shift of the jet in response to POLAR is smaller, when the two forcings are applied in tandem than when they are applied individually.

The jet strength response, seen in Figure 3.3b, also exhibits nonlinear behavior. As with the jet position response, the jet strength response is approximately linear in the winter and summer, and nonlinear in the transition seasons. Recall from Figure 3.2c that the jet strength response to POLAR is negative (a weakening of the jet) in every month, while the jet strength response to TROP is positive (a strengthening of the jet) from March through October, approximately zero in February/November, and negative in January/December. Thus, the overall sign of the jet strength response for the combined forcings also changes with season—in the colder months (ONDJFM), the net response for BOTH and for TROP + POLAR is a weakening of the jet, while the net response for the two experiments is positive (strengthening) in the summer. This suggests that the weakening of the jet driven by the POLAR heating is inhibited when POLAR is applied together with TROP, reducing the overall amplitude of the jet strength response.

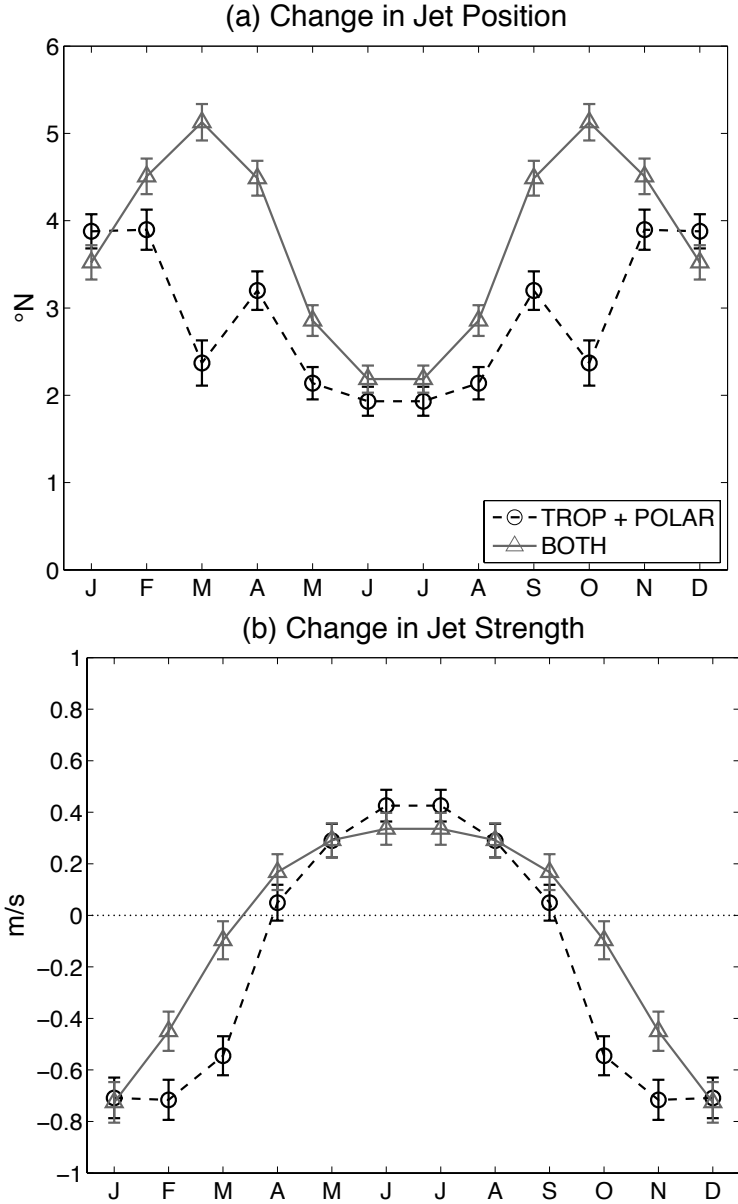


FIGURE 3.3. Change in (a) jet position and (b) jet strength for BOTH and TROP + POLAR heating experiments. Here, the error bars indicate the confidence bounds on the difference of means between BOTH and TROP+POLAR.

In addition to studying the nonlinearity of the jet response to heating in different locations, the circulation may also respond non-linearly to the amplitude of the heating. That is, for an incremental change in the strength of the heating ( $q_0$  in equation 2.5), is there an equivalent incremental change in the jet position and strength responses? To answer

this question, an additional set of simulations is performed under March/October conditions. March/October is chosen since it is the month with the most nonlinear responses to the upper tropical and lower polar warming (Figure 3.3). Both tropical upper tropospheric heatings and polar lower tropospheric heatings are applied individually, with the strength of the heating ( $q_0$ ) varying from -1.0 K/day to +1.0 K/day.

Figure 3.4 displays the mean jet position (Figure 3.4a) and strength (Figure 3.4b) responses as a function of heating strength for the TROP and POLAR heating experiments. Both the jet position and jet strength responses to the POLAR experiment are approximately linear, especially when the responses are further subdivided into heating ( $q_0 > 0$ ) and cooling ( $q_0 < 0$ ) experiments, as indicated by the dashed lines in Figure 3.4. However, the slopes of the best-fit lines are not identical for the heating and cooling experiments, implying some degree of nonlinearity.

The jet position and strength responses to the TROP experiment, however, are strongly nonlinear. The jet position response for heating amplitudes between  $\pm 0.2$  K/day varies greatly, from 32°N to 49°N. The jet position response for heating amplitudes outside of this range, however, is much more constrained. The response of the jet position is virtually flat for heating rates less than or equal to -0.4 K/day, and for heating rates greater than or equal to +0.8 K/day. Although a further exploration of the causes behind this behavior is beyond the scope of this work, previous studies have also suggested such limitations on the latitude of the eddy-driven jet. For example, Barnes et al. [4] discuss the importance of a turning latitude near the pole—that is, the inhibition of wave breaking on the poleward flank of a jet that is sufficiently poleward due to the decrease of  $\beta$  toward the pole. For more discussion

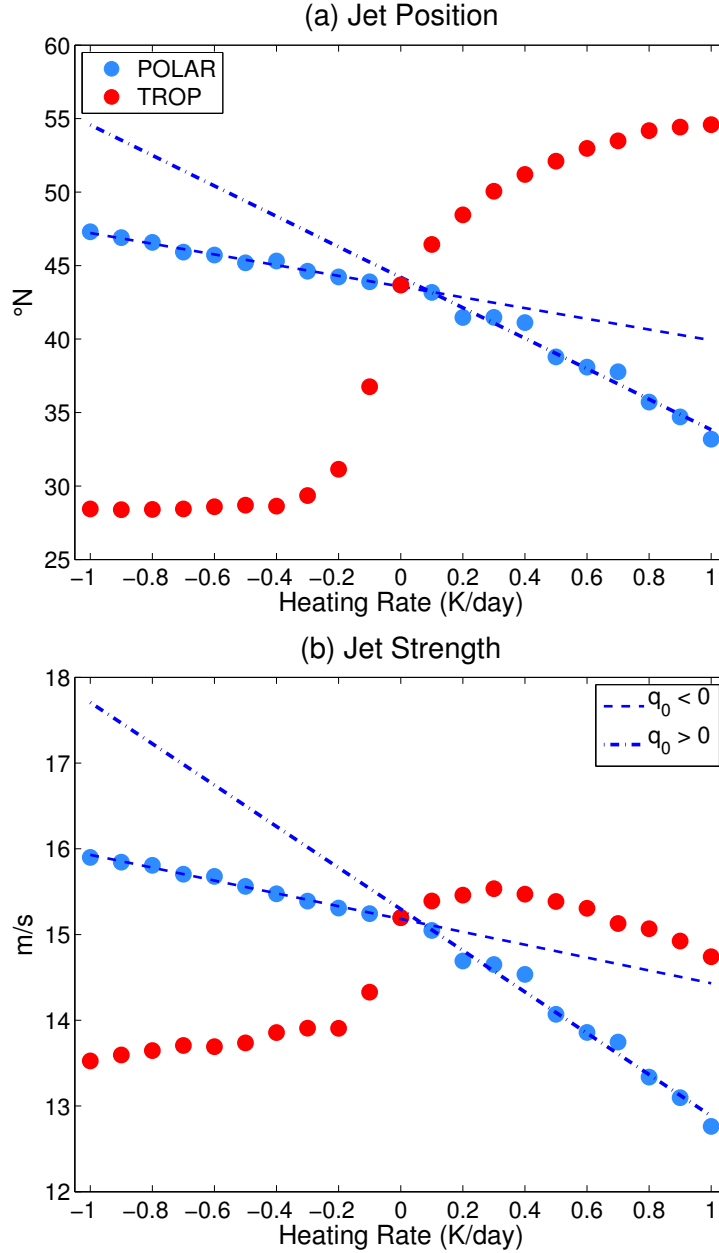


FIGURE 3.4. (a) Jet position and (b) jet strength as a function of heating rate in March/October. The lines indicates the best fit line for POLAR for values of  $q_0 \leq 0$  (dashed line) and  $q_0 \geq 0$  (dot-dash line).

of turning latitudes, see section 4 in Barnes et al. [4] and the references therein for a more thorough discussion of turning latitudes. It is possible that this inhibition of poleward wave breaking for a poleward shifted jet due to a reduction in the meridional gradient of planetary vorticity (that is,  $\partial_y \beta$  decreases going poleward) could act to inhibit further poleward

movement of the eddy-driven jet, thus explaining the asymptotic behavior around 54-55°N seen in Figure 3.4a.

There also appears to be an equatorward bound of the jet position seen in Figure 3.4a. One possibility is that the jet position is confined on the equatorward flank by the meridional extent of the subtropical circulation. For example, Figure 13 in Barnes and Hartmann [3] indicates that the relationship between the location of the “baroclinic zone” and the eddy-driven jet latitude in a barotropic model is not simply one-to-one—as the stirring latitude moves equatorward, the eddy-driven jet latitude moves less. Similarly, O’Rourke and Vallis [37] also demonstrate a minimum zonal phase speed bound that restricts the eddy activity to certain regions. Additionally, it is possible that the sharply asymptotic behavior exhibited by the jet position for  $q_0 \leq -0.4$  K is a result of the atmosphere becoming statically unstable due to the imposition of an upper-level cooling.

In Figure 3.4, as in Figure 3.2, the jet position and strength responses to the TROP experiment are not similar. For negative values of  $q_0$  in the TROP experiment (tropical upper level cooling), the jet appears to weaken as the amplitude of the cooling increases, although these changes are small for coolings larger than -0.2 K/day (Figure 3.4b). For small tropical upper level heatings ( $0 < q_0 \leq 0.3$  K/day), the jet strength increases with the heating amplitude. However, as the heating strength exceeds 0.3 K/day, the jet starts to weaken again with increasing heating strength. One possible explanation for this behavior is that in these strong tropical heating cases, the maximum meridional temperature gradient is shifted too far poleward, and out of midlatitudes, potentially inhibiting the formation of the eddy-driven jet by either weakening or removing the eddy heat fluxes that help the

eddy-driven jet form and maintain itself, or by moving the region of maximum eddy heat fluxes (the baroclinic region) into the polar regions, where spherical geometry inhibits the formation of the eddy-driven jet due to weak planetary vorticity gradients (see discussion in Butler et al. [9] for more).

As previously discussed, the jet position and strength responses to the POLAR heating are approximately linear over the range of heating amplitudes shown in Figure 3.4, and do not level off as is the case for TROP. One might wonder, what happens when the POLAR heating amplitude is increased beyond  $\pm 1.0\text{K/day}$ ? The circulation was further perturbed by several additional experiments with  $1 < |q_0| < 3 \text{ K/day}$ . The results of this extended heating experiment are shown in Figure 3.5.

Figure 3.5 indicates that the jet position begins to flatten out around the latitudes that the TROP response approaches (  $55^\circ\text{N}$  for  $q_0 = -3 \text{ K/day}$  and  $28^\circ\text{N}$  for  $q_0 = +3 \text{ K/day}$ ). However, even for  $q_0 = \pm 3 \text{ K/day}$ , the response to POLAR has not quite flattened out the way that the response to TROP has. So, even for large values of  $q_0$  for the POLAR experiment, the strongly nonlinear behavior exhibited by the response to the TROP experiment is not found until the POLAR heating amplitudes are increased well beyond  $\pm 1 \text{ K/day}$ .

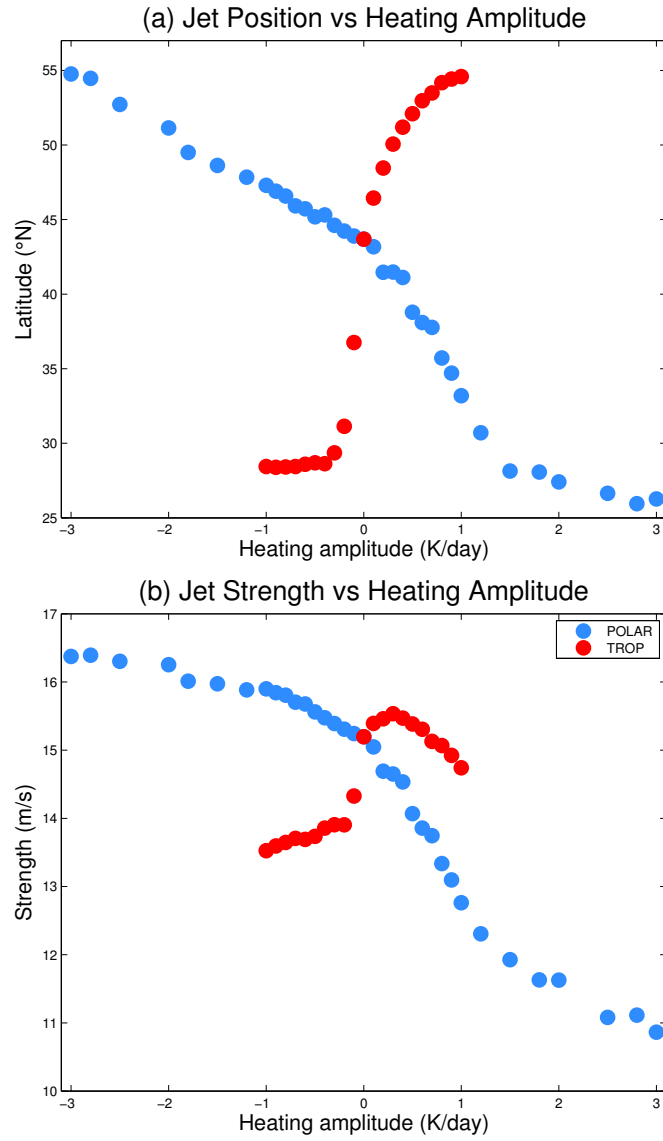


FIGURE 3.5. As in Figure 3.4, but for the extended values of heating amplitude ( $q_0$ ).

### 3.3. INITIAL JET POSITION EXPERIMENTS

The jet position response to an external forcing has been previously shown to be sensitive to the initial position of the jet. For example, Kidston and Gerber [30], Barnes and Hartmann [2], and Son et al. [49] all find that models with a more equatorward Southern Hemisphere jet exhibit an enhanced response to an external forcing, such as increased  $\text{CO}_2$  or loss of  $\text{O}_3$ . But does the sensitivity of the circulation to the basic state of the circulation, specifically the initial position of the jet, matter more in some seasons than in others? In this set of experiments, the seasonal sensitivity of the circulation response to the initial position of the jet is examined with the A+5, A+2, A-2, and A-5 experiments described in Section 2d. In observations, the eddy-driven jets are not all located at the same latitudes—the North Atlantic jet is generally located farther poleward than the North Pacific jet, for example. GCMs are also known to exhibit large equatorward biases in the jet position (e.g. Kidston and Gerber [30]). Therefore it is important to explore the seasonal sensitivity of the jet position response for jets with various initial positions.

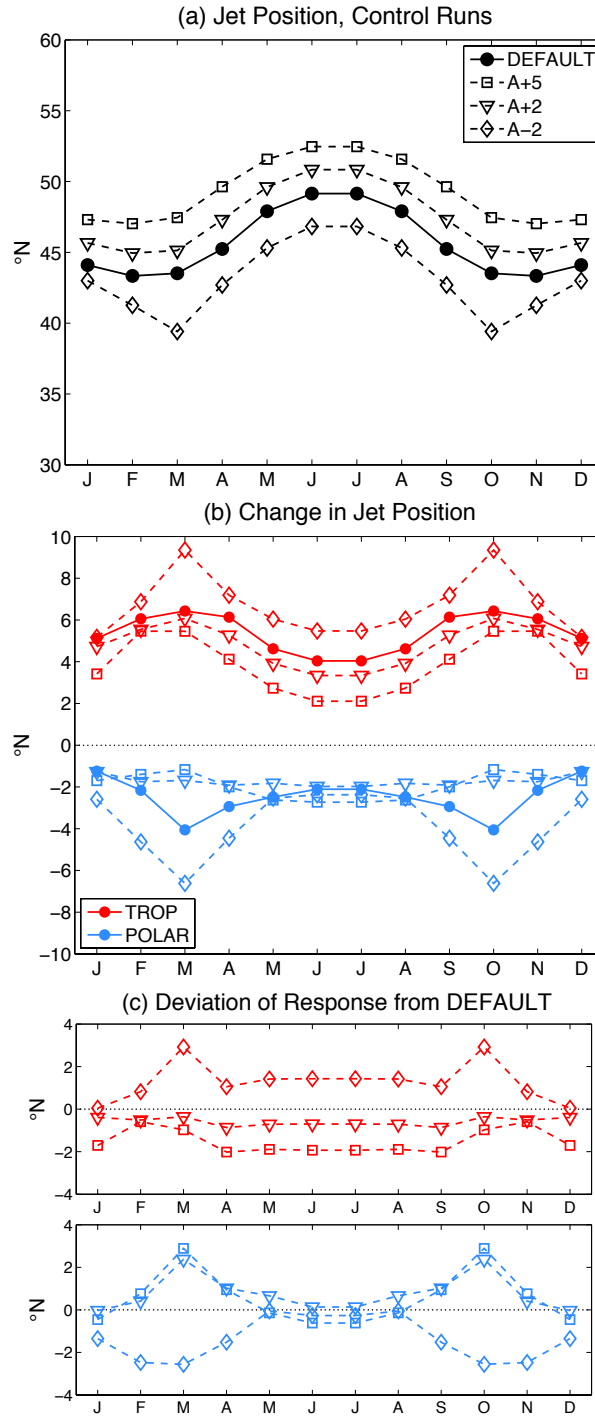


FIGURE 3.6. (a) Jet position for control runs, and (b) change in jet position for TROP and POLAR heating experiments for mean state experiments (A+5, A+2, and A-2) and model default (DEFAULT). (c) The difference in the jet position response for A+5, A+2, and A-2 compared to DEFAULT.

Figure 3.6a shows the jet position for the control runs for three mean state experiments (A+5, A+2, and A-2), and the model default configuration employed in the first set of experiments (referred to as DEFAULT). All four experiments in Figure 3.6a exhibit similar seasonal cycles of the jet position, with the jet furthest poleward in the summer and more equatorward in winter. The experiments simply shift the mean jet position—A+5 and A+2 have jets poleward of the jet position DEFAULT, while the A-2 jet is equatorward of the DEFAULT jet. A+5 and A+2 have jets with a slightly suppressed seasonal cycle when compared with that of DEFAULT, while the A-2 jet exhibits an enhanced seasonal cycle. A-5 (not shown) has a jet that is far equatorward of DEFAULT in all months, with a jet that shifts as far south as 30°N in the transition seasons. Additionally, the A-5 jet position in December-January is approximately the same as the A-5 jet position in June-July. This behavior is not seen in DEFAULT, or in A+5, A+2, or A-2, all of which have jets that are significantly more poleward in summer than in winter. As the seasonal cycle of the jet position in A-5 deviates substantially from that of DEFAULT, A-5 will not be discussed further.

The jet position response to the TROP and POLAR experiments for A+5, A+2, and A-2 are compared to the responses of DEFAULT in Figure 3.6b. All experiments in Figure 3.6 exhibit a poleward shift of the jet in response to a tropical upper tropospheric warming. Regardless of the initial jet position, this poleward shift is largest in the transition seasons, and smallest in the winter and summer. A-2, the jet position experiment with the most equatorward jet, exhibits the largest response to the TROP experiment, shifting nearly 10°N in March/October. A+5, the experiment with the most poleward jet, exhibits the weakest response to the TROP experiment, with a maximum response of around 5°. So, while the

magnitude of the jet response to tropical upper tropospheric heating does exhibit some dependence on the initial jet position, the overall seasonal sensitivity of the response appears at first glance to be similar, in that all four experiments peak in the transition seasons.

The four initial jet position experiments all exhibit an equatorward shift of the jet in response to the polar lower tropospheric warming (blue lines in Figure 3.6b). The response of A-2, the most equatorward jet position, exhibits a similar seasonality to the DEFAULT response to the POLAR experiment, with the strongest response in the transition seasons. As was the case for the TROP heating, A-2 also exhibits the largest response. However, the two mean states that have jets poleward of the DEFAULT jet, A+2 and A+5, do not exhibit the same seasonality in their responses to POLAR. The A+2 and A+5 responses appear to have little seasonality, with all months shifting 1.5-2° equatorward.

Is the jet response more sensitive to initial jet latitude in some months versus others? To more clearly visualize these results, the deviation of the mean state experiment responses (A+5, A+2, and A-2) from the DEFAULT responses to the TROP and POLAR experiments were calculated. That is, the A+5, A+2, and A-2 responses are subtracted from the DEFAULT responses to TROP and to POLAR, and these deviations are shown in Figure 3.6c. The deviations of the A+5 (red squares) and A+2 (red triangles) responses to the TROP heating experiment are approximately constant across all seasons, suggesting that the response is weakened by about the same amount compared to the DEFAULT response every month. The A-2 (red diamonds) response to the TROP experiment, however, does exhibit some seasonality. From April through September, the A-2 response is about 1.5° larger than the DEFAULT response to TROP. In March/October, however, the A-2 response is over

3° larger than the DEFAULT response to the same tropical heating. And from November through February, the A-2 response is nearly identical to the DEFAULT response to the TROP experiment.

The deviations of all three mean state experiment responses—A+5 (blue squares), A+2 (blue triangles), and A-2 (blue diamonds)—to the polar warming also exhibit a seasonality. All three experiments exhibit larger deviations from DEFAULT in the transition seasons compared to the winter and summer. In fact, the deviation for all three mean state experiments is approximately zero in the summer months. This is not to say the circulation response to a polar lower tropospheric warming is zero in the summer—Figure 3.6b shows that the jet shifts equatorward in MJJA around 2°. Rather, the mean state has little impact on the magnitude of this shift—no matter where the jet is initially located, it will shift equatorward about the same amount in response to a polar lower tropospheric warming in the summer months. Additionally, no matter where the jet is initially located, its response will deviate more from that of DEFAULT in the transition seasons—a reduction in the equatorward shift of the jet for the A+5 and A+2 experiments (jets poleward of DEFAULT), and an increase in the equatorward shift of the jet for the A-2 experiment (a jet equatorward of DEFAULT).

## CHAPTER 4

# SEASONALITY OF JET INTERNAL VARIABILITY

### 4.1. E-FOLDING TIME

Why is there such a strong seasonal sensitivity in the circulation response to tropospheric warming in these idealized experiments? Although a full exploration of this question is beyond the scope of this work, one possible mechanism that could explain the jet position response is discussed here. Namely, the seasonality of the circulation response is a manifestation of a seasonality of the low-frequency variability of the circulation of the control climate. This idea stems from the qualitative application of fluctuation-dissipation theory to climate change studies (see Gerber et al. [22], Shepherd [42]). In this context, fluctuation-dissipation theory suggests that the response of the atmosphere to an external perturbation is related to its internal variability. Specifically, larger internal variability will lead to a larger jet response that projects onto this variability. So, if the control simulations exhibit a greater jet variability in the transition seasons, one might expect these simulations to exhibit the largest response to thermal forcing in these seasons.

Following Gerber et al. [22], the e-folding time ( $\tau$ ) of the autocorrelation function of the first principal component time series of the zonal mean zonal wind at 775 hPa is used to characterize the low-frequency variability. The zonal mean, latitude-weighted zonal wind at 775 hPa ( $[U_{775}]$ ) from 20-70°N was calculated using daily data (note that the previous sections used 30-day mean data).  $\tau$  is defined as the e-folding time of the first principal component time series of the leading EOF of  $[U_{775}]$  (referred to as PC1).  $\tau$  is calculated by fitting a linear function to the autocorrelation function of PC1 around the approximate

value of  $\frac{1}{e}$ . This analysis was applied to each month of the unforced experiments (i.e., the control runs for DEFAULT, A+5, A+2, and A-2). Due to computational constraints, the previous experiments only output monthly data; however daily data were needed to calculate  $\tau$ . Therefore, two 8,640 day (24 year) runs for each value of  $\chi$  were run for each unforced experiment, outputting daily data. Approximately 7200 days were used to calculate each  $\tau$  after the first 1440 days (4 years) were discarded for spin-up. Using equation (2.3) of Gerber et al. [22], an integration length of 7200 days indicates that the standard deviation of  $\tau$  is likely less than one day for nearly all months of all experiments. The e-folding times for each simulation were calculated separately, and then the simulations using the same value of  $\chi$  were averaged together.

The values of  $\tau_{PC1}$  for all four unforced experiments, seen in Figure 4.1a, exhibit largely similar seasonal cycles to those of the jet position responses—the largest values of  $\tau_{PC1}$  occur in the transition seasons. In most months (all months in the A+2 and A+5 experiments), the e-folding times are under 25 days (thought to be the intrinsic autocorrelation timescale for variations in the extratropical jet in the Held-Suarez system, as described by Gerber et al. [22]). However, in the DEFAULT and A-2 runs (the experiments with the most equatorward initial jet positions), there are sharp increases in e-folding times in the transition months (February/November and March/October for A-2, and March/October for DEFAULT)—in these instances,  $\tau$  jumps as high as 85 days. These unrealistically large e-folding times have been previously documented (e.g. Gerber et al. [22]), and are likely attributable to persistent extreme events. For example, in the months with unrealistically high values of  $\tau$  ( $\tau > 30$  days), these persistent extremes (events with  $|PC1| > 2$ ) can up to 100 days (not shown).

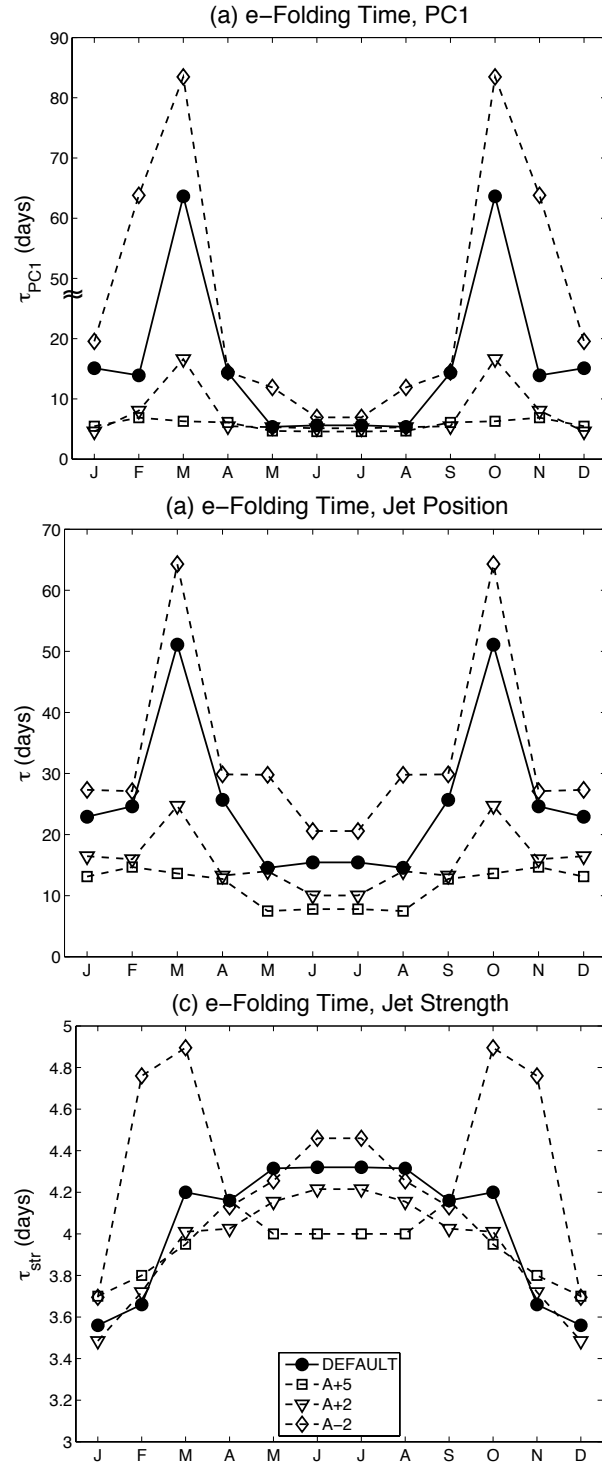


FIGURE 4.1. e-folding time ( $\tau$ ) for (a) PC1, (b) jet position, and (c) jet strength for model control runs. Note that the  $\tau$  scale for (a) skips from 20 to 50 days.

Next, the internal variability of the eddy-driven jet is decomposed further, by calculating the e-folding time of both the jet position and the jet strength independently. These separate e-folding times for jet position and jet strength can be seen in Figure 4.1b and 4.1c, respectively. The jet position e-folding time ( $\tau_{pos}$ , in Figure 4.1b) is generally higher in the transition seasons, and lower in summer and winter. The seasonal cycle of the jet position e-folding time is similar to the seasonal cycle of the e-folding time of PC1 (Figure 4.1a), and the seasonal cycle of the jet position response to heating (Figure 3.2b). Additionally, the jet position e-folding time is generally higher for the jets with more equatorward mean states (DEFAULT and A-2), which is in agreement with previous studies suggesting that equatorward jets are more persistent (e.g. Barnes et al. [4], Kidston and Gerber [30]). However, the high sensitivity of the e-folding timescales to extreme events remains—in March/October, the e-folding time of jet position jumps to about 50 days for DEFAULT, and about 65 days for A-2. The e-folding time of jet strength ( $\tau_{str}$  in Figure 4.1c) is generally higher in summer and lower in winter, following the seasonal cycle of the jet strength response to an upper tropical tropospheric heating (red circles in Figure 3.2c). Again, the e-folding time sharply increases in the transition seasons—this time, in February/November and March/October for A-2. Sharp increases in  $\tau_{str}$  are also seen in March/October for DEFAULT, although the summertime values of  $\tau_{str}$  are still larger for the DEFAULT experiment. So, while the  $\tau_{pos}$  and  $\tau_{PC1}$  exhibit similar seasonal sensitivities,  $\tau_{str}$  does not. Additionally, the extremely high values of  $\tau_{PC1}$  are likely driven by a combination of highly persistent variations of both jet latitude and jet speed. These results further suggest that jet position and jet strength should not be assumed to respond to forcing in the same way, as their variabilities do not exhibit the same seasonal cycles.

#### 4.2. SPREAD: A DIFFERENT METHOD OF QUANTIFYING INTERNAL VARIABILITY

As the e-folding calculation is clearly sensitive to extreme events, it is beneficial to quantify the internal variability of the circulation using another metric that is less sensitive to these extremes. The spread metric is defined as the difference between the 90th percentile and 10th percentile of a quantity—in this case, jet position and jet strength. Simply put, the jet position spread estimates the size of the range of latitudes over which the jet can be found on 80% of days, while the jet strength spread gives the range of strengths of the jet on 80% of days.

The jet position spread and jet strength spread can be seen in Figure 4.2a and Figure 4.2b, respectively. The jet position spread (Figure 4.2a) shares the same seasonal cycle as the jet position e-folding time (Figure 4.1b) and the jet position response to heating (Figure 3.2b). The jet position spread is greatest in the transition seasons, and lowest in the summer. Although the jet position spread is greatest in the transition seasons, it does not jump to extreme values the way  $\tau$  does. The jet strength spread, does not exhibit the same seasonal cycle as the jet strength response to heating (Figure 3.2c), or the jet strength e-folding time (Figure 4.1c). The jet strength spread is greatest in winter and lowest in summer in all experiments, and is also greatest for the more poleward initial jet positions (A+2 and A+5). The reason for this is clear—one possibility is that the poleward jets are generally less persistent (e.g. Barnes and Hartmann [2]), and therefore have less self-maintenance than their equatorward counterparts, thus accounting for a greater variability in jet strength. The A+2 and A+5 jets are stronger in every month than the DEFAULT and A-2 jets (not shown), so Figure 4.2b suggests that weaker jets have lower variability than stronger jets.

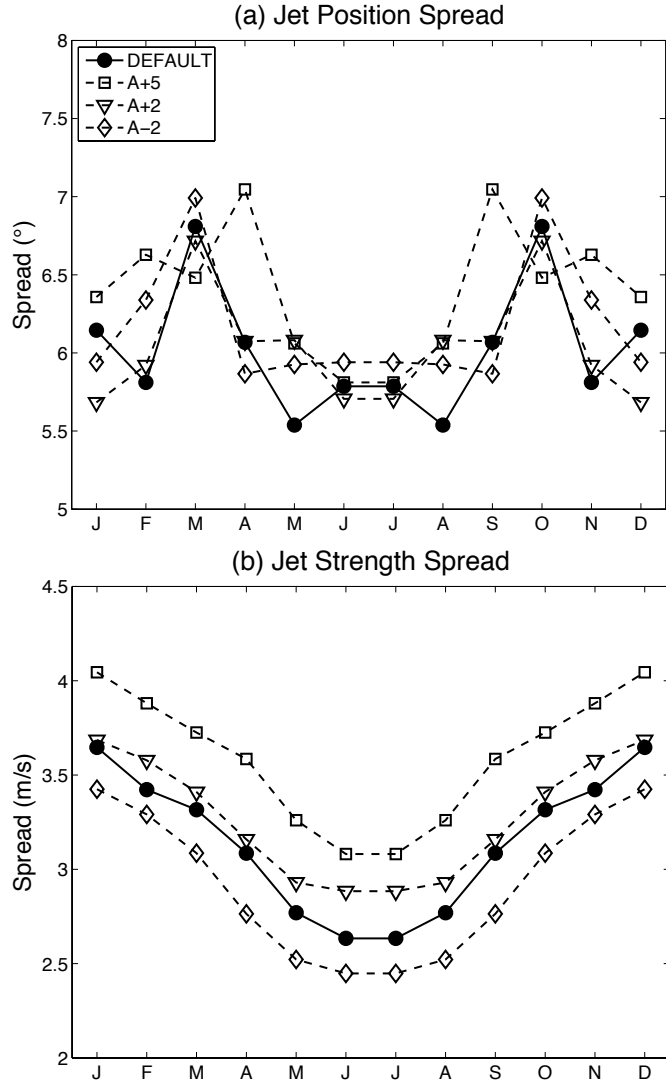


FIGURE 4.2. Spread for (a) jet position and (b) jet strength for model control runs.

Both the e-folding timescales and the jet position spreads suggest that the jet position response to anthropogenic forcing is greatest in months with the greatest internal variability—in this case, the transition seasons. The implications for the jet strength response are less clear. The jet strength e-folding timescales are generally greatest in the summer, matching the seasonal cycle of the jet strength response to tropical upper tropospheric warming (the TROP experiment). However, some experiments (A-2, and DEFAULT to a lesser extent) do exhibit sharp increases in jet strength e-folding times in the transition seasons, more

closely mirroring the seasonal cycle of the jet strength response to polar lower tropospheric warming (the POLAR experiment). These results suggest that the jet position response is well-correlated with the internal variability of the jet, although the jet strength response is less so.

### 4.3. COMPARISON WITH REANALYSIS

Finally, the e-folding time of the first principal component time series of the lower-level winds (PC1), and jet position and strength e-folding times are calculated for MERRA reanalysis data over the North Atlantic (defined as 15-75°N, 0-70°W) for comparison with the idealized model. These three quantities were computed for daily MERRA reanalysis data using the procedures described in section 2e. The North Atlantic is discussed here because the North Atlantic jet is considered to be primarily eddy-driven, while the North Pacific jet is both thermally driven and eddy-driven (e.g. Li and Wettstein [34], Eichelberger and Hartmann [18]). This analysis is not intended to quantify the extent to which the zonally symmetric idealized model results can emulate the observed variability of the North Atlantic jet. Rather, the aim for this analysis is to demonstrate that the internal variability of the observed eddy-driven jet also exhibits significant seasonality, and to show that the broad conclusions from these idealized modeling experiments do in fact have relevance to the future responses of the jets.

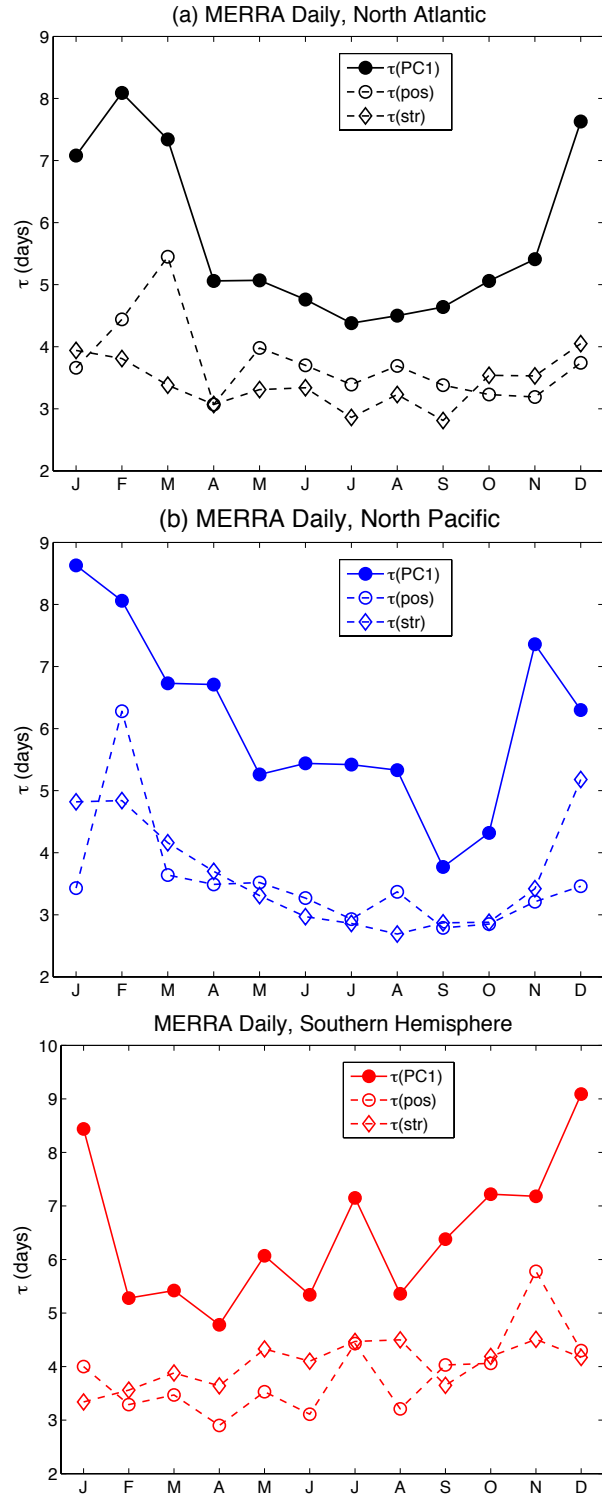


FIGURE 4.3. Jet position, jet strength, and PC1 e-folding times for daily MERRA reanalysis data for (a) the North Atlantic, (b) the North Pacific, and (c) the Southern Hemisphere.

Figure 4.3a displays the MERRA North Atlantic PC1 e-folding time (filled black circles), jet position e-folding time (open black circles), and jet strength e-folding time (open black diamonds). Figure 4.3a indicates that, as in the dry core results, the jet position and PC1 e-folding times for the North Atlantic reanalysis data display similar seasonal cycles, with both peaking in late winter/early spring, and decreasing in the summer. The contrast between winter and summer e-folding timescales is greater in  $\tau_{PC1}$  than it is in  $\tau_{pos}$ , with  $\tau_{PC1}$  reaching 7-8 days in December through March and remaining around 5 days the rest of the year, while  $\tau_{pos}$  only exceeds 4 days in February and March. The seasonal cycle of the jet strength e-folding time is flatter than those of  $\tau_{PC1}$  and  $\tau_{pos}$ , although  $\tau_{str}$  is slightly higher in the winter and lower in the summer.

The picture in the North Pacific (Figure 4.3b) and the Southern Hemisphere (Figure 4.3c) is more complicated.  $\tau_{PC1}$  has a clear seasonal cycle, maximizing around 8.5 days in January and reaching a minimum of about 4 days in September. The e-folding times of jet position ( $\tau_{pos}$ ) and jet strength ( $\tau_{str}$ ) have similar structures—they are generally largest in winter and smallest in summer. The Southern Hemisphere e-folding times (Figure 4.3c) actually demonstrates an opposite seasonality to the Northern Hemisphere e-folding times (Figure 4.3a and Figure 4.3b), with the greatest e-folding times for  $\tau_{PC1}$  occurring in Southern Hemisphere summer. The structure of  $\tau_{PC1}$  somewhat resembles that of  $\tau_{pos}$ , especially in Southern Hemisphere autumn and winter (AMJJAS).

Figure 4.3 indicates that the internal variability of the jets in the reanalysis data has a seasonal cycle, as does the internal variability of the model jets. Furthermore, these seasonalities are not the same across ocean basins, or across different physical quantities—that is,

the e-folding time of PC1 is not necessarily similar to the e-folding times of jet position and strength. So, while using the annular modes (i.e.  $\tau_{PC1}$ ) to quantify variability works well in some applications, the annular modes are ultimately amalgams of patterns of variability in both jet position and jet strength, and thus cannot necessarily be used to fully describe trends in jet position or jet strength. Although these idealized model results should not be interpreted as realistic, the dry dynamical core results can thus be used as a tool to provide insights regarding observations.

The mechanisms that explain the seasonal sensitivity of the jet response to these heating experiments are complex, and far from fully explored here. However, taken together, the seasonalities of the persistence of the jet's internal variability (e-folding time) and the jet position spread provide some insight into the circulation's seasonal sensitivity described in this paper. Generally speaking, the e-folding times and jet position spreads are greater in the spring and fall—the months that exhibit the largest jet position responses to tropospheric warming. This suggests that the internal variability of the unforced circulation may play at least some part in determining the seasonality of the jet position response—months with greater internal variability are more likely to exhibit a larger jet position response to an external heating. Regarding the jet strength response, as the seasonal sensitivities of the responses to the TROP and POLAR experiments are different, the response cannot be described by fluctuation-dissipation theory alone. Rather, while the seasonal cycle of internal variability may be able to explain the response to TROP, the jet speed response to POLAR does not resemble the response that would be predicted by fluctuation-dissipation.

## CHAPTER 5

# CONCLUSIONS

### 5.1. CONCLUSIONS

This study addresses the following questions: “What is the seasonal sensitivity of the circulation to tropospheric heating anomalies?”, and “How does the initial jet position impact the circulation’s seasonal sensitivity?”. The GFDL dry dynamical core is used to address these questions in an idealized framework. A seasonal cycle was applied in the model by adjusting the relaxation temperature profile to capture each month of the year. Two heating anomalies, a tropical upper tropospheric heating (TROP), and a polar lower tropospheric heating (POLAR) were applied to a variety of initial jet positions—the model default, and three adjusted jet positions (A+5, A+2, and A-2). The linearity of the circulation response to these thermal forcings was also assessed by applying both the TROP and POLAR experiments to the model default configuration simultaneously, and by adjusting the strengths of the individual TROP and POLAR experiments. With this suite of experiments, the seasonality of the circulation response to two identical heating profiles and the impact of the mean state of the circulation on these responses was explored. These experiments demonstrate that:

- (1) There is a seasonal sensitivity in the jet position response to identical forcing, with the transition seasons exhibiting the largest circulation response for both the TROP and POLAR experiments.
- (2) When forced with two heatings at once (TROP and POLAR), the circulation response is nonlinear in the transition seasons, and approximately linear in the winter and the summer.

- (3) In March/October, the months of the most nonlinear circulation response to multiple heating sources, the circulation response to the strength of the POLAR heating is approximately linear over the range of  $\pm 1$  K/day. However, the circulation response to the strength of the TROP heating over the same range is nonlinear.
- (4) The seasonal sensitivity of the circulation response to the TROP experiment is greatest in the transition seasons regardless of the initial jet position. The seasonal sensitivity of the circulation response to the POLAR experiment, however, does exhibit dependence on the initial jet position, with more poleward jets displaying less seasonal sensitivity than more equatorward jets in response to the POLAR experiment.
- (5) The months with the greatest jet position response are also the months with the greatest internal variability, suggesting that fluctuation-dissipation theory may explain, at least qualitatively, the jet position response to forcing. The relationship between the internal variability and the jet strength response is less clear.

Although these results were obtained in the very idealized environment of a dry dynamical core, the importance of the seasonality of the circulation should be considered in more realistic models and in observations. This study has shown that relatively minor changes to the circulation, such as those brought on by a seasonal cycle, can have large impacts on the circulation response even when only dry dynamics are considered. Even though the real world circulation exhibits seasonality driven by additional factors (e.g. land-sea contrast, stratospheric variability) not represented here, when evaluated in the context of climate variability and climate change, these results suggest that:

- (1) The sign of the jet position response to a tropical upper tropospheric heating (TROP) and a polar lower tropospheric heating (POLAR) is robust across all twelve

months of the year, shifting poleward in response to a tropical upper level heating, and equatorward in response to a polar lower level heating. However, the magnitude of this response varies with season. Thus, studies looking only at one particular season, or the annual mean, may underestimate or overestimate the responses in other seasons.

- (2) The importance of the initial jet position on the amplitude of the response highlights the importance of correctly modeling the mean state of the jet in the GCMs in order to fully estimate the magnitude and seasonality of the circulation response. Previous studies have noted an equatorward bias in jet latitude in climate models (e.g. Kidston and Gerber [30], Barnes and Polvani [5]), with more equatorward jets shifting more than their poleward counterparts. The results presented here are in agreement with these studies. However, these results highlight that the importance of this bias is not necessarily the same across seasons.
- (3) The circulation response to the simultaneously applied TROP and POLAR experiments is not linear in all seasons. Therefore, model simulations with only one forcing may obtain very different results than what might occur under climate change, although this depends on the season. In some seasons, the circulation response may be approximately linear, and the full circulation response can be assumed to be a simple superposition of the responses to the individual heatings.

## 5.2. FUTURE WORK

5.2.1. MODELING EXPERIMENTS. The work presented here should not be viewed only as a set of idealized modeling results, but also as a set of experiments that can be applied to a hierarchy of models. The seasonal sensitivity experiments outlined here can be run using a

series of increasingly physically complex models. In this way, the changes in the seasonality of the response due to the addition of more physical mechanisms can be examined. For example, Frierson et al. [20] describe a simplified moist general circulation model (GCM) that is similar to the Held-Suarez dry dynamical core used in this thesis. This model utilizes an ocean surface to provide a moist evaporative flux into the atmosphere, and a gray radiation scheme that does not account for the effects of water vapor on radiation. This model can be used with convective scheme that improves the strength and width of the Hadley cell when compared to that of the dry model (see Frierson [19] for more). Running the experiments described in this thesis in the moist GCM would provide a better environment for exploring the relationship between the seasonality of the eddy-driven jet and the seasonality of the subtropical jet strength and position. Many current hypotheses regarding the dynamical mechanisms driving the eddy-driven jet response attribute at least some of the response to the state of the subtropical circulation. Son and Lee [48] suggest that the subtropical jet strength controls the location of the baroclinic region; Garfinkel et al. [21] show that the magnitude of the eddy-driven jet response to the stratospheric vortex strength depends on the distance between the eddy-driven jet and the subtropical jet; and Eichelberger and Hartmann [18] and Barnes and Hartmann [3] both demonstrate that the eddy-driven jet variability (which is coupled to the eddy-driven jet response via fluctuation-dissipation theorem) is dependent on the position and strength of the subtropical jet. Additionally, many studies have shown a relationship between the observed eddy-driven jets and subtropical jets, particularly in the North Pacific (e.g. Lee and Kim [33], Nakamura and Sampe [36], Li and Wettstein [34]). A better understanding of the impact of the subtropical circulation on the seasonality of

the midlatitude jet response to climate change could facilitate better understanding of observed variability, and of trends in the midlatitude jet response in the state-of-the-art GCMs.

Similarly, this framework could be applied to models with increasing complexity in other areas. For example, recent studies (e.g. Ceppi et al. [10], Ceppi et al. [11], Grise and Polvani [24], Li et al. [35]) have highlighted the importance of cloud radiative effects on the midlatitude circulation. Ceppi et al. [10] link biases in top of atmosphere shortwave cloud radiative forcing to biases in the position of the Southern Hemisphere jet; Grise and Polvani [24] and Ceppi et al. [11] both suggest that trends in the top of atmosphere cloud radiative effects in CMIP5 models are associated with trends in the midlatitude jets; and Li et al. [35] explore the impacts of cloud radiative effects on the atmospheric circulation in an atmospheric general circulation model (AGCM). The seasonality of the circulation response to an idealized cloud radiative heating profile (as in Figure 4 of Li et al. [35]) could be explored using this same framework in the dry core. Although it may seem counterintuitive to explore the effects of cloud radiative heating in a dry model, the experiments described here prescribe an unvarying heating profile, and allow the circulation to respond accordingly—they use a dry model to explore the dry dynamical response to cloud radiative heating. Alternatively, another method of exploring the impact of cloud radiative forcing on the seasonality of the circulation might be to use the cloud and vapor-locking technique described in Voigt and Shaw [55]. This technique essentially turns the CMIP5 aquaplanet models into simplified moist GCMs that include latent heat release but do not include radiative effects.

The work presented in this thesis explores only the zonally symmetric component of the circulation response to climate change. However, significant zonal asymmetries exist in the real circulation, particularly in the Northern Hemisphere. These zonal asymmetries are

the result of differences in stationary wave patterns, caused by topographic features, and differences in land-sea contrast. Recently, it has been shown that the zonally asymmetric midlatitude circulation response to climate change in the CMIP5 models is quite complex, with changes in the stationary wave patterns being associated with changes in the eddy-driven jet position (e.g. Simpson et al. [46], Brandefelt and Körnich [7]). Simpson et al. [46] hypothesize that the seasonality in the response of the midlatitude circulation to climate change is driven by changes in the stationary wave pattern; this hypothesis could perhaps be tested using the experiments described here and including realistic topography in the dry model.

This work also suggests that the jet position and jet strength responses to anthropogenic forcing cannot be assumed to be the same (see Figure 3.2). This point has also been made recently in other works—Thomas et al. [52] show that the natural variability of the jet strength, jet position, and Southern Annular Mode (SAM) are not the same in the CMIP5 models, and Swart et al. [50] show that the trends in the Southern Hemisphere eddy-driven jet and the SAM are not the same in the CMIP5 models or in 20th century reanalysis. It is not known, however, why the jet strength and position responses are different. Perhaps there is some seasonality in the strength and/or position of the maximum baroclinic region (given by the maximum of  $\frac{\partial T}{\partial y}$ )? Or perhaps the shape of the zonal-mean zonal wind profile changes slightly, giving a broader but ultimately slightly weaker peak for the eddy-driven jet strength, which might indicate a weakening trend? As this study calculates jet strength by fitting a simple polynomial through the maximum point of  $[U]$ , it is possible that this metric is missing this kind of change.

5.2.2. VARIABILITY IN REANALYSIS. In analyzing the MERRA reanalysis data for the final part of this thesis, it became clear that a study of the seasonal cycles of internal variability (or even the seasonal cycles of jet position and strength) of the various real-world eddy-driven jets does not currently exist. The internal variability metrics used in this idealized study could be further applied to observations and to more realistic models. The purpose of such a study would be twofold. The first goal is to formally record and quantify the seasonal cycles of jet position, strength, and internal variability of the observed eddy-driven jets (see Figure 1.1 and Figure 4.3). The second is to use the CMIP5 models (the state-of-the-art GCMs) to quantify the seasonal cycle of jet internal variability for each model, and to explore the relationship between the seasonal cycles of jet internal variability, and jet response to forcing under the RCP8.5 (high emission) and RCP4.5 (moderate emission) scenarios. In this way, some of the conclusions from this thesis can be tested in more realistic GCMs.

## REFERENCES

- [1] Barnes, E. A., N. W. Barnes, and L. M. Polvani, 2013: Delayed Southern Hemisphere climate change induced by stratospheric ozone recovery, as projected by the CMIP5 models. *J. Clim.*, **27**, 852–867, doi:10.1175/JCLI-D-13-00246.1.
- [2] Barnes, E. A., and D. L. Hartmann, 2010: Testing a theory for the effect of latitude on the persistence of eddy-driven jets using CMIP3 simulations. *Geophys. Res. Lett.*, **37**, L15 801, doi:10.1029/2010GL044144.
- [3] Barnes, E. A., and D. L. Hartmann, 2011: Rossby wave scales, propagation, and the variability of eddy-driven jets. *J. Atmos. Sci.*, **68**, 2893–2908, doi:10.1175/JAS-D-11-039.1.
- [4] Barnes, E. A., D. L. Hartmann, D. M. W. Frierson, and J. Kidston, 2010: Effect of latitude on the persistence of eddy-driven jets. *Geophys. Res. Lett.*, **37**, L11 804, doi:10.1029/2010GL043199.
- [5] Barnes, E. A., and L. M. Polvani, 2013: Response of the midlatitude jets and of their variability to increased greenhouse gases in the CMIP5 models. *J. Climate*, **26**, 7117–7135.
- [6] Barnes, E. A., and D. W. J. Thompson, 2014: Comparing the roles of barotropic versus baroclinic feedbacks in the atmosphere’s response to mechanical forcing. *J. Atmos. Sci.*, **71**, 177–194.
- [7] Brandefelt, J., and H. Körnich, 2008: Northern hemisphere stationary waves in future climate projections. *J. Clim.*, **21**, 6341–6353, doi:10.1175/2008JCLI2373.1.
- [8] Butler, A. H., D. W. J. Thompson, and T. Birner, 2011: Isentropic slopes, down-gradient eddy fluxes, and the extratropical atmospheric circulation response to tropical tropospheric heating. *J. Atmos. Sci.*, **68**, 2292–2305, doi:10.1175/JAS-D-10-05025.1.

- [9] Butler, A. H., D. W. J. Thompson, and R. Heikes, 2010: The steady-state atmospheric circulation response to climate change-like thermal forcings in a simple general circulation model. *J. Climate*, **23**, 3474–3496.
- [10] Ceppi, P., Y.-T. Hwang, D. M. W. Frierson, and D. L. Hartmann, 2012: Southern Hemisphere jet latitude biases in CMIP5 models linked to shortwave cloud forcing. *Geophys. Res. Lett.*, **39**, L19 708, doi:10.1029/2012GL053115.
- [11] Ceppi, P., D. Zelinka, and D. L. Hartmann, 2014: The response of the Southern Hemispheric eddy-driven jet to future changes in shortwave radiation in CMIP5. *Geophys. Res. Lett.*, **41**, 3244–3250, doi:10.1029/2014GL060043.
- [12] Chen, G., and I. M. Held, 2007: Phase speed spectra and the recent poleward shift of southern hemisphere surface westerlies. *Geophys. Res. Lett.*, **34**, L21 805, doi:10.1029/2007GL031200.
- [13] Chen, G., and R. A. Plumb, 2014: Effective isentropic diffusivity of tropospheric transport. *J. Atmos. Sci.*, **71**, 3499–3520, doi:10.1175/JAS-D-13-0333.1.
- [14] Collins, M., and Coauthors, 2013: Long-term Climate Change: Projections, Commitments and Irreversibility. In: *Climate Change 2013: The Physical Science Basis. Contribution of Working Group I to the Fifth Assessment Report of the Intergovernmental Panel on Climate Change*. Cambridge University Press.
- [15] Davis, N. A., and T. Birner, 2013: Seasonal to multi-decadal variability of the width of the tropical belt. *J. Geophys. Res.*, **118**, 7773–7787, doi:10.1002/jgrd.50610.
- [16] Deser, C., R. Tomas, M. Alexander, and D. Lawrence, 2010: The seasonal atmospheric response to projected Arctic sea ice loss in the late twenty-first century. *J. Clim.*, **23**, 333–351.

- [17] Deser, C., R. A. Tomas, and L. Sun, 2015: The role of ocean-atmosphere coupling in the zonal-mean atmospheric response to Arctic sea ice loss. *J. Clim.*, **28**, 2168–2186, doi:10.1175/JCLI-D-14-00325.1.
- [18] Eichelberger, S. J., and D. L. Hartmann, 2007: Zonal jet structure and the leading mode of variability. *J. Clim.*, **20**, 5149–5163.
- [19] Frierson, D. M. W., 2007: The dynamics of idealized convection schemes and their effect on the zonally averaged tropical circulation. *J. Atmos. Sci.*, **64**, 1959–1976.
- [20] Frierson, D. M. W., I. M. Held, and P. Zurita-Gotor, 2006: A gray-radiation aquaplanet moist GCM, part I: Static stability and eddy scales. *J. Atmos. Sci.*, **63**, 2548–2566.
- [21] Garfinkel, C. I., D. W. Waugh, and E. P. Gerber, 2013: The effect of tropospheric jet latitude on coupling between the stratospheric polar vortex and the troposphere. *J. Climate*, **26**, 2077–2095.
- [22] Gerber, E. P., S. Voronin, and L. M. Polvani, 2008: Testing the annular mode autocorrelation time scale in simple atmospheric general circulation models. *Mon. Wea. Rev.*, **136**, 123–1536.
- [23] Gillett, N. P., and J. C. Fyfe, 2013: Annular mode changes in the CMIP5 simulations. *Geophys. Res. Lett.*, **40**, 1189–1193, doi:10.1002/grl.50249.
- [24] Grise, K. M., and L. M. Polvani, 2014: Southern Hemisphere cloud dynamics biases in CMIP5 models and their implications for climate projections. *J. Clim.*, **27**, 6074–6092.
- [25] Hannachi, A., E. A. Barnes, and T. Woollings, 2013: Behaviour of the winter North Atlantic eddy-driven jet stream in the CMIP3 integrations. *Clim. Dyn.*, **41**, doi:doi:10.1007/s00382-012-1560-4.

- [26] Harvey, B. J., L. C. Shaffrey, and T. J. Woollings, 2014: Equator-to-pole temperature differences and the extra-tropical storm track responses of the CMIP5 climate models. *Clim. Dyn.*, **43**, 1171–1182, doi:10.1007/s00382-013-1883-9.
- [27] Held, I. M., 1993: Large-scale dynamics and global warming. *Bull. Amer. Meteor. Soc.*, **74**, 228–241, doi:10.1175/1520-0477(1993)074<0228:LSDAGW>2.0.CO;2.
- [28] Held, I. M., and M. J. Suarez, 1994: A proposal for the intercomparison of the dynamical cores of atmospheric general circulation models. *Bull. Am. Meteorol. Soc.*, **75**, 1825–1830.
- [29] Holland, M. M., and C. M. Bitz, 2003: Polar amplification of climate change in coupled models. *Clim. Dyn.*, **21**, 221–232.
- [30] Kidston, J., and E. P. Gerber, 2010: Intermodel variability of the poleward shift of the austral jet stream in the CMIP3 integrations linked to biases in the 20th century climatology. *Geophys. Res. Lett.*, **37**, L09 708, doi:10.1029/2010GL042873.
- [31] Kushner, P. J., and L. M. Polvani, 2004: Stratosphere-troposphere coupling in a relatively simple AGCM: The role of eddies. *J. Clim.*, **17**, 629–639.
- [32] Kushner, P. J., and L. M. Polvani, 2006: Stratosphere-troposphere coupling in a relatively simple AGCM: Impact of the seasonal cycle. *J. Climate*, **19**, 5721–5727.
- [33] Lee, S., and H.-K. Kim, 2003: The dynamical relationship between subtropical and eddy-driven jets. *J. Atmos. Sci.*, **60**, 1490–1503.
- [34] Li, C., and J. J. Wettstein, 2012: Thermally drive and eddy-driven jet variability in reanalysis. *J. Clim.*, **25**, 1587–1596.
- [35] Li, Y., D. W. J. Thompson, and S. Bony, 2015: The influence of atmospheric cloud radiative effects on the large-scale atmospheric circulation. *J. Clim.*, **28**, 7263–7278, doi:10.1175/JCLI-D-14-00825.1.

- [36] Nakamura, H., and T. Sampe, 2002: Trapping of synoptic-scale disturbances into the North-Pacific subtropical jet core in midwinter. *Geophys. Res. Lett.*, **29**, doi:10.1029/2002GL015535.
- [37] O'Rourke, A. K., and G. K. Vallis, 2013: Jet interaction and the influence of a minimum phase speed bound on the propagation of eddies. *J. Atmos. Sci.*, **70**, 2614–2628, doi:10.1175/JAS-D-12-0303.1.
- [38] Polvani, L. M., and P. J. Kushner, 2002: Tropospheric response to stratospheric perturbations in a relatively simple general circulation model. *Geophys. Res. Lett.*, **29**, 1114, doi:10.1029/2001GL014284.
- [39] Rienecker, M. M., and Coauthors, 2011: MERRA: NASA's Modern-Era Retrospective Analysis for Research and Applications. *J. Clim.*, **24**, 3624–3648.
- [40] Ring, M. J., and R. A. Plumb, 2008: The response of a simplified GCM to axisymmetric forcings: Applicability of the fluctuation-dissipation theorem. *J. Atmos. Sci.*, **65**, 3880–3898.
- [41] Screen, J. A., and I. Simmonds, 2010: The central role of diminishing sea ice in recent Arctic temperature amplification. *Nature*, **464**, 1334–1337.
- [42] Shepherd, T. G., 2014: Atmospheric circulation as a source of uncertainty in climate change projections. *Nature Geosci.*, **7**, 703–708, doi:10.1038/ngeo2253.
- [43] Sheshadri, A., R. A. Plumb, and E. P. Gerber, 2015: Seasonal variability of the polar stratospheric vortex in an idealized AGCM with varying tropospheric wave forcing. *J. Atmos. Sci.*, **72**, 2248–2266, doi:10.1175/JAS-D-14-0191.1.
- [44] Simpson, I. R., M. Blackburn, J. Haigh, and S. Sparrow, 2010: The impact of the state of the troposphere on the response to stratospheric heating in a simplified GCM. *J. Climate*, **23**, 6166–6185.

- [45] Simpson, I. R., M. Blackburn, and J. D. Haigh, 2012: A mechanism for the effect of tropospheric jet structure on the annular mode-like response to stratospheric forcing. *J. Atmos. Sci.*, **69**, 2152–2170, doi:10.1175/JAS-D-11-0188.1.
- [46] Simpson, I. R., T. A. Shaw, and R. Seager, 2014: A diagnosis of the seasonally and longitudinally varying midlatitude circulation response to global warming. *J. Atmos. Sci.*, **71**, 2489–2515, doi:10.1775/JAS-D-13-0325.1.
- [47] Simpson, I. R., T. G. Shepherd, P. Hitchcock, and J. F. Scinocca, 2013: Southern Annular Mode dynamics in observations and models. Part II: eddy feedbacks. *J. Clim.*, **26**, 5220–5241, doi:10.1175/JCLI-D-12-00495.1.
- [48] Son, S.-W., and S. Lee, 2005: The response of the westerly jets to thermal driving in a primitive equation model. *J. Atmos. Sci.*, **62**, 3741–3757.
- [49] Son, S.-W., and Coauthors, 2010: Impact of stratospheric ozone on Southern Hemisphere circulation change: A multimodel assessment. *J. Geophys. Res.*, **115**, D00M07, doi:10.1029/2010JD014271.
- [50] Swart, N. C., J. C. Fyfe, N. Gillett, and G. J. Marshall, in press: Comparing trends in the Southern Annular Mode and surface westerly jet. *J. Clim.*, doi:10.1175/JCLI-D-15-0334.1.
- [51] Tandon, N. F., L. M. Polvani, and S. M. Davis, 2011: The response of the tropospheric circulation to water vapor-like forcings. *J. Clim.*, **24**, 5713–5720, doi:10.1175/JCLI-D-11-00069.1.
- [52] Thomas, J. L., D. W. Waugh, and A. Gnanadesikan, 2015: Southern Hemisphere extratropical circulation: Recent trends and natural variability. *Geophys. Res. Lett.*, **42**, 5508–5515, doi:10.1002/2015GL064521.

- [53] Thompson, D. W. J., and T. Birner, 2012: On the linkages between the tropospheric isentropic slope and eddy fluxes of heat during Northern Hemisphere Winter. *J. Atmos. Sci.*, **69**, 1811–1823, doi:10.1175/JAS-D-11-0187.1.
- [54] Thompson, D. W. J., and S. Solomon, 2002: Interpretation of recent Southern Hemisphere climate change. *Science*, **296**, 895–899.
- [55] Voigt, A., and T. A. Shaw, 2015: Circulation response to warming shaped by radiative changes of clouds and water vapour. *Nature Geosci.*, **8**, 102–106, doi:10.1038/ngeo2345.
- [56] Wang, S., E. P. Gerber, and L. M. Polvani, 2012: Abrupt circulation responses to tropical upper-tropospheric warming in a relatively simple stratosphere-resolving AGCM. *J. Clim.*, **25**, 4097–4115.
- [57] Williams, L. N., S. Lee, and S.-W. Son, 2006: Dynamics of the Southern Hemisphere spiral jet. *J. Atmos. Sci.*, **64**, 548–563.
- [58] Woollings, T., A. Hannachi, and B. Hoskins, 2010: Variability of the North Atlantic eddy-driven jet stream. *Quart. J. Roy. Meteor. Soc.*, **136**, 856–868, doi:10.1002/qj.625.
- [59] Yin, J. H., 2005: A consistent poleward shift of the storm tracks in simulations of 21st century climate. *Geophys. Res. Lett.*, **32**, L18 701, doi:10.1029/2005GL023684.